



Cloud and aerosol  
classification for 2  
1/2 years of  
MAX-DOAS  
observations

Y. Wang et al.

# Cloud and aerosol classification for 2 1/2 years of MAX-DOAS observations in Wuxi (China) and comparison to independent data sets

Y. Wang<sup>1,2</sup>, M. Penning de Vries<sup>1</sup>, P. H. Xie<sup>2</sup>, S. Beirle<sup>1</sup>, S. Dörner<sup>1</sup>, J. Remmers<sup>1</sup>, A. Li<sup>2</sup>, and T. Wagner<sup>1</sup>

<sup>1</sup>Max Planck Institute for Chemistry, Hahn-Meitner-Weg 1, 55128 Mainz, Germany

<sup>2</sup>Anhui Institute of Optics and Fine Mechanics, Chinese Academy of Sciences, Hefei, China

Received: 31 March 2015 – Accepted: 20 April 2015 – Published: 6 May 2015

Correspondence to: Y. Wang (y.wang@mpic.de)

Published by Copernicus Publications on behalf of the European Geosciences Union.

Title Page

Abstract

Introduction

Conclusions

References

Tables

Figures



Back

Close

Full Screen / Esc

Printer-friendly Version

Interactive Discussion



## Abstract

Multi-Axis-Differential Optical Absorption Spectroscopy (MAX-DOAS) observations of trace gases can be strongly influenced by clouds and aerosols. Thus it is important to identify clouds and characterise their properties. In a recent study Wagner et al. (2014) developed a cloud classification scheme based on the MAX-DOAS measurements themselves with which different “sky conditions” (e.g. clear sky, continuous clouds, broken clouds) can be distinguished. Here we apply this scheme to long term MAX-DOAS measurements from 2011 to 2013 in Wuxi, China (31.57° N, 120.31° E). The original algorithm has been modified, in particular in order to account for smaller solar zenith angles (SZA). Instrumental degradation is accounted for to avoid artificial trends of the cloud classification. We compared the results of the MAX-DOAS cloud classification scheme to several independent measurements: aerosol optical depth from a nearby AERONET station and from MODIS, visibility derived from a visibility meter; and various cloud parameters from different satellite instruments (MODIS, OMI, and GOME-2). The most important findings from these comparisons are: (1) most cases characterized as clear sky with low or high aerosol load were associated with the respective AOD ranges obtained by AERONET and MODIS, (2) the observed dependences of MAX-DOAS results on cloud optical thickness and effective cloud fraction from satellite indicate that the cloud classification scheme is sensitive to cloud (optical) properties, (3) separation of cloudy scenes by cloud pressure shows that the MAX-DOAS cloud classification scheme is also capable of detecting high clouds, (4) some clear sky conditions, especially with high aerosol load, classified from MAX-DOAS observations corresponding to the optically thin and low clouds derived by satellite observations probably indicate that the satellite cloud products contain valuable information on aerosols.

## Cloud and aerosol classification for 2 1/2 years of MAX-DOAS observations

Y. Wang et al.

Title Page

Abstract

Introduction

Conclusions

References

Tables

Figures

◀

▶

◀

▶

Back

Close

Full Screen / Esc

Printer-friendly Version

Interactive Discussion



## 1 Introduction

In the last decade, Multi-Axis- (MAX-) Differential Optical Absorption Spectroscopy (DOAS) has received considerable attention due to its application to the retrieval of vertical distributions of trace gases and aerosols (Hönninger et al., 2004; Bobrowski et al., 2003; Pikelnaya et al., 2007; Sinreich et al., 2007; Theys et al., 2007; Clémer et al., 2009, 2010; Wagner et al., 2011; Vlemmix et al., 2010, 2011, 2015). Scattered sunlight spectra recorded by MAX-DOAS instruments at multiple elevation angles are analysed using DOAS (Platt and Stutz, 2008) to acquire slant column densities (SCDs) of several trace gases; the slant column density represents the trace gas concentration integrated along the atmospheric light path. Different inversion approaches, e.g. based on look up tables or optimal estimation, are applied to derive tropospheric profiles of trace gases and aerosols from the measured SCDs (e.g. Wittrock et al., 2004; Wagner et al., 2004, 2011; Heckel et al., 2005; Frieß et al., 2006, 2011; Irie et al., 2008, 2011; Clémer et al., 2010; Li et al., 2010, 2012; Yilmaz, 2012; Vlemmix et al., 2015). Cloud-free sky is an ideal condition for the profile inversion, whereas under cloudy skies the atmospheric light paths are complicated, especially for rapidly changing cloud conditions. In principle it would be possible to include clouds in the radiative transfer simulations, but usually the necessary information on cloud properties is not available (e.g. Erle et al., 1995; Wagner et al., 1998, 2002, 2004; Winterrath et al., 1999). So it is important to identify and classify clouds and aerosols for each measurement in order to characterise the quality of the measurement result. In this study, we refer to the presence and properties of clouds and aerosols as “sky conditions”. Cloud information derived from MAX-DOAS observations – instead of other sources like e.g. visual inspection or camera images – is very important, because it can be directly assigned to individual MAX-DOAS observations without any spatio-temporal interpolation and without requiring the installation of additional instrumentation. This will become especially important for harmonized MAX-DOAS data processing in global monitoring networks of tropospheric species in the future.

## Cloud and aerosol classification for 2 1/2 years of MAX-DOAS observations

Y. Wang et al.

Title Page

Abstract

Introduction

Conclusions

References

Tables

Figures

◀

▶

◀

▶

Back

Close

Full Screen / Esc

Printer-friendly Version

Interactive Discussion





## Cloud and aerosol classification for 2 1/2 years of MAX-DOAS observations

Y. Wang et al.

Title Page

Abstract

Introduction

Conclusions

References

Tables

Figures

◀

▶

◀

▶

Back

Close

Full Screen / Esc

Printer-friendly Version

Interactive Discussion



by MAX-DOAS are compared to cloud and aerosol information from a variety of independent ground-based and satellite instruments, such as the Aerosol Robotic Network (AERONET) (Holben et al., 1998, 2001), a visibility meter, the Ozone Monitoring instrument (OMI) (Levelt et al., 2006a, b), the Global Ozone Monitoring Experiment (GOME-2) (Callies et al., 2000; Munro et al., 2006) and the two MODerate Resolution Imaging Spectroradiometer (MODIS) instruments (<http://modis.gsfc.nasa.gov/>) (Kaufmann et al., 2002).

The paper is organized as follows: in Sect. 2 we describe the properties of the MAX-DOAS instrument in Wuxi, China and the retrieval of the quantities used for the cloud classification. Then we describe the principles and procedures to adapt and improve the automatic cloud classification scheme. We also introduce the independent datasets used for comparison. Section 3 presents the results of identified sky conditions and their comparisons with independent data sets. In Sect. 4 the discussion and conclusions are given.

## 2 Datasets and methods

### 2.1 MAX-DOAS instrument

A Mini-MAX-DOAS instrument (Li et al., 2007) is automatically operated and taken care of by the Wuxi Chinese Academy of Sciences Photonics corporation on the roof of a 11-story building in Wuxi City, China (31.57° N, 120.31° E, 50 m a.s.l.) from May 2011 to present. The data in the period until November 2013 are included in this work, except for the time between 15 December 2011 to 28 February 2012, when the instrument was not in operation. The instrument is designed to sequentially acquire scattered sunlight spectra at different elevation angles (the angle between the horizon and the viewing direction). The indoor computer controls the acquisition of spectra and pointing of the telescope. All the outdoor components are protected by a metal sealed box consisting of the entrance optics and a light-weight fiber coupled spectrometer cooled by a Peltier

**Cloud and aerosol  
classification for 2  
1/2 years of  
MAX-DOAS  
observations**

Y. Wang et al.

Title Page

Abstract

Introduction

Conclusions

References

Tables

Figures

◀

▶

◀

▶

Back

Close

Full Screen / Esc

Printer-friendly Version

Interactive Discussion

element. In the entrance optics a stepper motor controls the elevation angles. The entrance optics consists of a quartz lens coupled to a quartz fiber bundle which leads the collected light into the spectrograph. The entrance optics has a field-of-view (FOV) of  $\sim 0.4^\circ$ . The light is dispersed by a crossed Czerny–Turner spectrometer (HR2000+, Ocean Optics Inc.) with a spectral resolution of 0.35 nm over a spectral range from 290–425 nm. A one-dimensional Charge Coupled Device (CCD) is used as the detector. During the observation period the instrument was pointed exactly into the north direction and performed measurements at sequences of five elevation angles (5, 10, 20, 30 and  $90^\circ$ ). A full elevation sequence usually took about 12 min depending on the received radiance. The CCD exposure time is automatically adjusted based on the scattered solar radiance to ensure  $\sim 70\%$  of the saturation level of the detector. 100 individual scans are averaged for each elevation angle to enhance the signal to noise ratio. For the measurement of background spectra (containing dark current and electronic offset) a light shade in the entrance optics is used. Individual background spectra are subtracted from the corresponding measured spectra to correct dark current and electronic offset. In this study only measurements for solar zenith angle (SZA)  $< 90^\circ$  are considered.

## 2.2 Quantities from MAX-DOAS observations

The cloud/aerosol classification is based on three quantities retrieved from the MAX-DOAS measurements: (1) radiance (indicating the brightness of the sky), (2) a color index (CI), i.e. the ratio of radiances at two wavelengths (indicating the color of the sky), and (3) the spectral absorption of the oxygen dimer (indicating changes of the atmospheric light paths, e.g. multiple scattering). Different sky conditions are defined by comparing these quantities and their temporal variation to threshold values, as in Wagner et al. (2014).

In the following sections, we will introduce each of the quantities and discuss their particularities. In particular, it has to be carefully elaborated how stable the instrument is



**Cloud and aerosol  
classification for 2  
1/2 years of  
MAX-DOAS  
observations**

Y. Wang et al.

Title Page

Abstract

Introduction

Conclusions

References

Tables

Figures

◀

▶

◀

▶

Back

Close

Full Screen / Esc

Printer-friendly Version

Interactive Discussion



for the calibration. We assumed an aerosol layer from the surface to 1 km, an asymmetry parameter of 0.68, a single scattering albedo of 0.95, an Angström parameter of 1.0 and a surface albedo of 5%. We used a slightly different AOD (0.14 at 440 nm; Wagner et al. (2014) used 0.24), as this value was measured at the nearby AERONET station Taihu (see Fig. 2a). The radiative transfer simulations using the RTM McArtim (Deutschmann et al., 2011) are performed for the SZA range of 1–90° in steps of 1°. In Fig. 3 the CI and the radiance on the three clear days are compared to the corresponding radiative transfer simulation results (please note the different y axes on the left and right side of the figures). For the CI good agreement of the SZA dependencies is found (see Fig. 3a). Thus the calibration of the CI is simply performed by multiplication of the measured values with a proportionality constant  $\alpha$ , which in our case is 0.89. In contrast to the CI, the SZA dependence of the measured and modeled radiances does not agree as well: for SZA < 40 measured radiances are much larger than the modeled radiances. This systematic difference is probably caused by the deviation of the true aerosol phase function from the Henyey–Greenstein parameterization (Henyey and Greenstein, 1941) used in the model simulations. For this reason, we determined the proportionality constant for the calibration of the radiance in the SZA interval between 50 and 81° (note that no measurements at SZA > 81° were available during the selected days). We derived a proportionality constant of  $7.01 \times 10^{-7}$  counts<sup>-1</sup>.

Because the large discrepancy of the radiances for SZA < 40° between measurements and simulations, the clear sky reference radiances for the whole SZA interval, which are needed for the normalization, cannot be taken from model calculations, we took an empirical approach. First, we fitted a polynomial to the measured radiances (green line in Fig. 3b). Because no measurements for SZA < 12° were available, a method to extrapolate the clear sky reference radiances to smaller SZA had to be found. Our first idea was to simply extend the fitted polynomial to SZA < 12° (see green curve in Fig. 4). However, because of the strong dependence of the polynomial for small SZA the corresponding errors would be quite large. Instead we decided to choose the average of the maximum and minimum radiances measured for all sky conditions (see



column density (VCD, the vertically integrated concentration) (Solomon et al., 1987):

$$\text{AMF} = \frac{\text{SCD}}{\text{VCD}}. \quad (2)$$

The  $\text{O}_4$  concentration is proportional to the square of the  $\text{O}_2$  concentration (Greenblatt et al., 1990) and thus varies only slightly with time (due to variations of temperature and pressure). Thus for the conversion to AMF we used a constant  $\text{VCD}_{\text{O}_4}$  of  $1.25 \times 10^{43}$  molecules<sup>2</sup> cm<sup>-5</sup> (for the unit see Greenblatt et al., 1990). This value is calculated from average values of the surface temperature (290 K) and surface pressure (1010 hPa) at Wuxi. Here it should be noted that during the course of one year we found deviations of the  $\text{O}_4$  VCD from the selected value of  $\pm 10\%$ . Since in this study we use the  $\text{O}_4$  measurements only for the identification of fog (see below), these deviations don't have an effect on the cloud primary classification results. Also the effect of the fog classification is very small

For the interpretation of the  $\text{O}_4$  AMF, another important aspect has to be considered: to remove the strong solar Fraunhofer lines, usually a FRS is included in a DOAS fit. Since the FRS used in our analysis is also taken from the MAX-DOAS measurements, i.e. also contains atmospheric  $\text{O}_4$  absorption, the  $\text{O}_4$  SCDs derived from the DOAS fit actually represent the differences between the  $\text{O}_4$  SCDs of both the measured spectra and the FRS. This difference is usually referred to as differential SCDs (dSCD). Like the  $\text{O}_4$  SCDs (Eq. 2), also the  $\text{O}_4$  dSCD can be converted into the corresponding  $\text{O}_4$  dAMF:

$$\text{dAMF}_{\text{O}_4} = \frac{\text{dSCD}_{\text{O}_4}}{\text{VCD}_{\text{O}_4}}. \quad (3)$$

We also investigate the effect of the instrumental degradation on the  $\text{O}_4$  dSCD. We find systematic temporal variations of  $\text{O}_4$  dSCD (see Fig. S1a in the Supplement) are probably caused by changes of the spectral resolution of the instrument (see Fig. S1b

Cloud and aerosol classification for 2 1/2 years of MAX-DOAS observations

Y. Wang et al.

Title Page

Abstract

Introduction

Conclusions

References

Tables

Figures

◀

▶

◀

▶

Back

Close

Full Screen / Esc

Printer-friendly Version

Interactive Discussion



## Cloud and aerosol classification for 2 1/2 years of MAX-DOAS observations

Y. Wang et al.

Title Page

Abstract

Introduction

Conclusions

References

Tables

Figures

◀

▶

◀

▶

Back

Close

Full Screen / Esc

Printer-friendly Version

Interactive Discussion



in the Supplement). Because of the systematic variations we did not use the  $O_4$  absorption measured in zenith for the identification of optically thick clouds. Instead we identify optically thick clouds by largely reduced values of the measured radiances.

Wagner et al. (2014) used measurements of the  $O_4$  absorption also for the identification of fog. In the presence of fog, almost the same  $O_4$  absorption is observed for all elevation angles. Since this particular test requires only the comparison of  $O_4$  absorption within a single elevation sequence, it is independent of instrument degradations and the use of individual FRS per elevation sequence is not critical.

### 2.3 The scheme of the classification of sky conditions

Wagner et al. (2014) investigated the sensitivity of several quantities, listed in Table 1, derived from MAX-DOAS observations to the presence and properties of clouds and aerosols and proposed a cloud classification scheme. From this scheme, in addition to the identification of clear and cloudy skies, further parameters like high and low aerosol optical depth (AOD), optically thin or thick clouds, continuous or broken clouds, or fog can be retrieved. The determination criteria of both the schemes introduced in this paper and in Wagner et al. (2014) are presented in Table 2.

#### 2.3.1 General principles and construction of the classification scheme

The classification scheme is based on the CI, radiance and  $O_4$  absorption derived from MAX-DOAS as described in Sect. 2.2. Wagner et al. (2014) did sensitivity studies of the quantities with respect to the properties of clouds and aerosols. The basic classification results are derived from the retrieved CI for zenith observations: compared to clear sky conditions, the CI is systematically decreased in the presence of clouds. Also the temporal variation of the CI is investigated, because in the presence of clouds usually substantial temporal variations of the CI occur. They can be quantified by the so called

temporal smoothness indicator (TSI), the discretized second derivative in time:

$$\text{TSI}_{y,n} = 2 \cdot \left[ \frac{\Delta t_1 y_{n+1} + \Delta t_2 y_{n-1}}{\Delta t_1 \Delta t_2 \cdot (\Delta t_1 + \Delta t_2)} - \frac{y_n}{\Delta t_1 \Delta t_2} \right]. \quad (4)$$

Here  $y$  is the CI and  $n$  indicates the number of the selected elevation sequence,  $\Delta t_1$  and  $\Delta t_2$  are the time steps between measurement sequences  $n - 1$  and  $n$ ,  $n$  and  $n + 1$ , respectively. The TSI can be calculated for all elevation angles separately. In this study,  $\text{TSI}_z$  refers to the TSI for the measurements in zenith view, and  $\text{TSI}_L$  to the sum of the TSI for all non-zenith elevation angles.

The spread of the CI for different elevation angles is also investigated: in the presence of clouds, usually similar CI values are found for all elevation angles, whereas for clear sky conditions, the CI values for different elevation angles differ significantly. The spread is quantified by the difference between the maximum and minimum CI for all elevation angles in one elevation sequence.

In addition to the CI, the  $\text{O}_4$  absorption (expressed as  $\text{O}_4$  dAMF, see Eq. 3) is investigated: the  $\text{O}_4$  dAMF for zenith observation increases strongly in the presence of optically thick clouds. In addition, usually similar  $\text{O}_4$  absorption values for different elevation angles are found in the presence of fog.

The measured radiance is used in the cloud classification scheme for the identification of optically thick clouds: while optically thin clouds cause an increased radiance, in the presence of optically thick clouds the radiance is largely reduced.

All quantities used in this study and their acronyms are listed in Table 1. Based on these quantities the classification scheme of clouds and aerosols is constructed and its determination criteria are shown in Table 2. Most sky conditions are exclusive, that means that only one condition can be fulfilled at a given time; we refer to them in the following as primary sky conditions. The other conditions, “fog” and “optically thick clouds”, indicate additional information, and are referred to as secondary sky conditions. In Table 2, the symbol “&” requires that two criteria are simultaneously fulfilled, whereas “or” means that at least one of both criteria is fulfilled.

**Cloud and aerosol  
classification for 2  
1/2 years of  
MAX-DOAS  
observations**

Y. Wang et al.

Title Page

Abstract

Introduction

Conclusions

References

Tables

Figures

◀

▶

◀

▶

Back

Close

Full Screen / Esc

Printer-friendly Version

Interactive Discussion



### 2.3.2 Description of the adapted scheme

The modifications from the Wagner et al. (2014) scheme that we apply to make the scheme more suitable to the observation site and the instrument are as follows:

- a. The thresholds of different quantities, used for the cloud classification, listed in Table 1, are adapted to the specific properties of the MAX-DOAS instrument in Wuxi. A detailed description of the procedure of the selection of thresholds can be found in the Supplement. Because of the different clear sky reference values of CI and radiances, we modified the thresholds for CI and radiances in this study compared to Wagner et al. (2014). In addition, the threshold values of  $TSI_z$  and  $TSI_l$  had to be adapted due to the instrument-specific response to the spectral radiance. The different sets of elevation angles within one measurement sequence also require different thresholds for the spread value of CI. In Table 1, our thresholds are compared to those used in Wagner et al. (2014).
- b. The calibration and normalisation of the radiance is extended to the lower boundary of SZA of  $10^\circ$ , corresponding to the lower latitude of Wuxi compared to Cabauw (see Sect. 2.2.1).
- c. As outlined above, in this study we only consider the spread of the  $O_4$  dAMF (difference between the maximum and minimum values of the dAMFs in an elevation sequence) to identify the presence of fog. We did not use the  $O_4$  absorption for the detection of optically thick clouds, but rather detected them using the measured radiance (see Sect. 2.2.2 and Table 2).
- d. Two additional categories are included in the scheme which are not part of the Wagner et al. (2014) algorithm (Table 2): first, we found that at small SZA (which did not occur during the Cabauw measurements used by Wagner et al., 2014) the discrimination of cloudy conditions from clear conditions based on zenith measurements of the CI, especially in the case of continuous clouds, is no longer

## Cloud and aerosol classification for 2 1/2 years of MAX-DOAS observations

Y. Wang et al.

Title Page

Abstract

Introduction

Conclusions

References

Tables

Figures

◀

▶

◀

▶

Back

Close

Full Screen / Esc

Printer-friendly Version

Interactive Discussion





in Wagner et al. (2014) should not be used. An additional indicator is needed to detect the presence of continuous clouds.

Fortunately, the spread of the CI for the different elevation angles ( $\text{spread}_{\text{CI}}$ ) can be used for that purpose. In Fig. 7, it is shown that during the whole day  $\text{spread}_{\text{CI}}$  is lower than its threshold indicating the presence of continuous clouds. Whenever such a situation is encountered, the sky condition is denoted as “continuous clouds (small SZA)” to separate it from the “regular” continuous cloud detection, which is denoted as “continuous clouds (large SZA)”.

### 2.3.4 Exceptional case: extremely high midday CI

On six days, all classified as “clear with low aerosol load”, another interesting phenomenon was found: in the course of the day, the normalised CI increases until it peaks far above the threshold between 1 and 2 p.m. LT, whereas the normalised radiance drops below the threshold. In contrast to the findings for continuous clouds at small SZA, the spread of the CI remains above the threshold (see results for 29 July 2012, Fig. 8). The latter finding clearly indicates that no continuous clouds were present on that day. This conclusion is confirmed by the MODIS true color images (Fig. 9a), where no clouds can be seen. In Fig. 9b two measured radiance spectra for similar SZA (about  $20^\circ$ ) and their ratio are shown. At wavelengths larger than 330 nm, much lower intensities are measured in the afternoon (red spectrum) than in the morning (black), and the ratio between both spectra depends linearly on wavelength, decreasing from 1 at about 320 nm to 0.7 at 420 nm. At the time of writing, we can only speculate on the causes of this phenomenon. We focus on three possible explanations.

1. The findings are artifacts related to measurement geometry. The fact that this exceptional case was only encountered in summer and only within a small time range (1–2 p.m.) suggests an influence of SZA, perhaps similar to the case found for continuous clouds at very small SZA. However, the peak in CI and corresponding dip in normalized radiance do not occur at the smallest SZA.

## Cloud and aerosol classification for 2 1/2 years of MAX-DOAS observations

Y. Wang et al.

Title Page

Abstract

Introduction

Conclusions

References

Tables

Figures

◀

▶

◀

▶

Back

Close

Full Screen / Esc

Printer-friendly Version

Interactive Discussion





and aerosols. An automatic cloud screening scheme is applied to the level 1.0 data to yield the largely cloud-cleared level 1.5 data set (Smirnov et al., 2000).

A forward-scattering visibility meter (Manufacturer: Anhui Landun Photoelectron Co. Ltd. Model: DNQ2 forward-scattering visibility meters) was operated near the MAX-DOAS instrument at the Wuxi site. This visibility meter automatically measures the visibility at 550 nm derived from the forward-scattered signal of a light-emitting diode at 950 nm using an empirical conversion formula (Nebuloni, 2005).

## 2.4.2 OMI and GOME-2 cloud products

The OMI (Levelt et al., 2006a and 2006b) aboard the EOS Aura satellite achieves daily global coverage. Its spatial resolution is 24 km × 13 km in nadir, and increases to 68 km × 14 km at the swath edges (disregarding the outer 5 pixels). The OMI overpass above the Wuxi site is between 13:00 and 14:00 LT. Effective cloud fraction (CF) and cloud top pressure (CP) retrieved from OMI are extracted from OMCLDO2 product, DOMINO version 2.0 (Acarreta et al., 2004; Sneep et al., 2008) obtained from the Tropospheric Emission Monitoring Internet Service (TEMIS) (<http://www.temis.nl>). The cloud products from OMI are retrieved using the O<sub>4</sub> absorption band at 477 nm. The effective CF is the cloud fraction of a Lambertian cloud with albedo 0.8 yielding the same top-of-atmosphere (TOA) radiance as the real cloud in the scene (Stammes et al., 2008). For the comparisons with the MAX-DOAS results, only data for satellite ground pixel centers with a distance less than 0.1° latitude and 0.2° longitude from the Wuxi site are included. In addition, the observations of the outermost pixels (i.e. pixel numbers 1–10 and 51–60) or pixels where a “row anomaly” had been reported (see [http://www.temis.nl/docs/omi\\_warning.html](http://www.temis.nl/docs/omi_warning.html)) were removed before the comparison (see also Ma et al., 2013).

The Meteorological Operational satellite platform (METOP-A) (Callies et al., 2000; Munro et al., 2006) was launched in October 2006 in a sun-synchronous polar orbit with an equator crossing time of 09:30 LT. It carries the GOME-2 with a spatial resolution of 80 km × 40 km and a global coverage in 1.5 days. We obtained the effective CF

## Cloud and aerosol classification for 2 1/2 years of MAX-DOAS observations

Y. Wang et al.

Title Page

Abstract

Introduction

Conclusions

References

Tables

Figures

◀

▶

◀

▶

Back

Close

Full Screen / Esc

Printer-friendly Version

Interactive Discussion



## Cloud and aerosol classification for 2 1/2 years of MAX-DOAS observations

Y. Wang et al.

Title Page

Abstract

Introduction

Conclusions

References

Tables

Figures

◀

▶

◀

▶

Back

Close

Full Screen / Esc

Printer-friendly Version

Interactive Discussion

and the CP from the daily level 2 products of the TM4NO2A version 2.3 (Boersma et al., 2004) from the TEMIS website. The effective CF and the CP are retrieved by the improved Fast Retrieval Scheme for Clouds from the Oxygen A-band algorithm (FRESCO+) (Wang et al., 2008) based on the measurements of the O<sub>2</sub> A-band around 760 nm. Considering the rather coarse spatial resolution of GOME-2, to keep as much data as possible, the selection criterion was extended to a distance within 0.2° latitude and 0.4° longitude from the Wuxi site.

### 2.4.3 Images, aerosol and cloud products from MODIS

Two MODIS instruments are operated on the Terra and Aqua satellites. They provide radiance images from which various products can be retrieved. In this study we use operational level 2 cloud products (Baum and Platnick, 2006). Terra and Aqua operate in polar sun-synchronous orbits at 705 km above the Earth's surface with a daytime equator crossing at 10.30 a.m. and 1.30 p.m. LT, respectively. Considering that the MAX-DOAS measurements are only analysed for daytime, we just extracted daytime cloud products from MODIS.

Two MODIS aerosol product clusters (MOD04\_L2 from Terra and MYD04\_L2 from Aqua) and two MODIS Level 2 cloud product clusters (MOD06\_L2 from the Terra platform and MYD06\_L2 from the Aqua platform) are acquired from collection 5.1 supplied by NASA (<http://ladsweb.nascom.nasa.gov/data/search.html>). We used the AOD at 550 nm with the spatial resolution of 10 km × 10 km from the scientific data set of “Optical\_Depth\_Land\_And\_Ocean”, which has more stringent control, namely requires that the quality assurance confidence (QAC) flag be larger than 0 over land (see Levy et al., 2010 and Remer et al., 2005). A technique known as CO<sub>2</sub> slicing is used to deduce the CP and the geometrical CF from radiances measured in the spectral bands located within the broad 15 μm CO<sub>2</sub> absorption region (Wielicki and Coakley, 1981) at 5 km × 5 km resolution. The cloud optical thickness (COT) is retrieved by the solar reflectance technique at a visible wavelength (e.g., 0.65 μm) and a shortwave-infrared (SWIR) wavelength (e.g., 1.64 or 2.15 μm) based on the decision tree algorithm (Plat-

nick et al., 2003; King et al., 2004). COT is given at 1 km × 1 km resolution. As for OMI, MODIS data with ground pixel centers within 0.1° latitude and 0.2° longitude from the Wuxi site are included for the comparison with MAX-DOAS.

In addition to the MODIS aerosol and cloud products, for selected case studies we also used true color images above Taihu (near the Wuxi site) with a spatial resolution of 250 m derived from both MODIS instruments. They were downloaded from the website of MODIS Rapid Response, NASA/GSFC ([http://aeronet.gsfc.nasa.gov/cgi-bin/bamgomas\\_interactive](http://aeronet.gsfc.nasa.gov/cgi-bin/bamgomas_interactive)). The true color images give an intuitive view of the coverage and structure of the clouds and aerosols over Wuxi.

The effective CF from OMI and GOME-2 is not a geometrical CF as retrieved by MODIS, but it is a combination of geometric CF, cloud reflectance, and clear sky reflectance (see Eq. 5). To make the cloud products more comparable, we converted the MODIS level 2 cloud optical thickness ( $\tau_c$ ), which is given at 650 nm (King et al., 1998), into an observed TOA cloud reflectance  $R(\tau_c)$ , and computed the effective CF ( $CF_{\text{eff}}$ ) from the cloud reflectance and geometric CF ( $CF_{\text{geo}}$ ) in a similar way as Stammes et al. (2008):

$$CF_{\text{eff}} = CF_{\text{geo}} \frac{R(\tau_c) - R_{\text{clear}}}{R_{\text{alb}=0.8} - R_{\text{clear}}}, \quad (5)$$

where  $R_{\text{clear}}$  is the clear sky reflectance, and  $R_{\text{alb}=0.8}$  is the reflectance of the clouds with cloud albedo of 0.8. The relation of  $R(\tau_c)$  and COT is acquired by simulations using McArtim and is shown in Fig. S2 in the Supplement. Note that the occurrence of effective CF larger than 1 is possible due to the fact that cloud albedo may be larger than 0.8. (Stammes et al., 2008). However we set the effective CF from MODIS to 1 if the calculated effective CF is larger than 1, because the effective CF from OMI and GOME-2 is also clipped between 0 and 1 (Wang et al., 2008).

## Cloud and aerosol classification for 2 1/2 years of MAX-DOAS observations

Y. Wang et al.

Title Page

Abstract

Introduction

Conclusions

References

Tables

Figures

◀

▶

◀

▶

Back

Close

Full Screen / Esc

Printer-friendly Version

Interactive Discussion



### 3 Results

#### 3.1 Cloud classification results for 2 1/2 years of MAX-DOAS measurements

The monthly mean relative frequency and monthly accumulated observation numbers of the different sky conditions from MAX-DOAS are shown in Fig. 10. Figure 10b indicates that more observations were made in summer because of the longer duration of the days and due to the shorter exposure time for individual measurements. The gap from 15 December 2012 to 28 February 2013 is caused by a temporal shutdown of the MAX-DOAS instrument. The short-term shutdowns in July and August 2013 also affect the number of observations.

An obvious intra-annual variation of the frequencies of clear sky and cloudy conditions can be found in Fig. 10a. The frequency of the clear sky conditions is higher in winter than in summer, especially with high aerosol load. The frequency of cloudy skies is higher in summer than in winter, especially of continuous clouds. This annual variation of the cloud amount over the Yangtze River Delta, China, including Wuxi station, has been reported by Zhao et al. (2014). The continuous clouds (small SZA) only occur in summer, which is due to the fact that these are only found for small SZA (below about  $35^\circ$ , see Sect. 2.3.3). However, we cannot exclude the possibility that part of the seasonal variation might be caused by the dependence on SZA of the retrieved cloud sensitive parameters.

An overview on the relative fraction of occurrences of the different sky conditions for the complete measurement time series is presented in Fig. 11. Cloudy skies including “continuous clouds (large SZA)”, “continuous clouds (small SZA)”, “broken clouds” and “cloud holes” were present in the majority of measurements (about 80.4%). “Broken clouds”, “cloud holes” in zenith or off-zenith view, and continuous clouds (“continuous clouds (high SZA)” and “continuous cloud (low SZA)”) account for about 62, 31 and 27% of all cloudy skies, respectively. The category “continuous clouds (small SZA)” contributes only about 19% to the continuous clouds. “Optically thick clouds” accounts for 14.1% of the cloudy cases. 50.0, 33.1 and 16.9% of “optically thick clouds” are as-

## Cloud and aerosol classification for 2 1/2 years of MAX-DOAS observations

Y. Wang et al.

Title Page

Abstract

Introduction

Conclusions

References

Tables

Figures

◀

▶

◀

▶

Back

Close

Full Screen / Esc

Printer-friendly Version

Interactive Discussion



signed to the sky conditions of “continuous clouds (high SZA)”, “continuous clouds (low SZA)” and “broken clouds”, respectively. Clear skies including either low or high aerosol load were present in about 19 % of all measurements. “Extremely high midday CI” was only present in 0.3 % of all measurements. The remaining 25 % of all measurements is classified as “cloud holes” in zenith or off-zenith view.

## 3.2 Comparison with coincident ground-based and satellite measurements

In this section we compare the results of our cloud classification scheme for the whole time period with coincident data from the independent data sets (AOD from AERONET and MODIS, visibility from visibility meter and cloud products from MODIS, OMI and GOME-2). Our general procedure is to firstly assign the MAX-DOAS results to each data point from the independent measurements and then to determine the absolute numbers and the relative fractions of the individual sky conditions for different intervals of the quantities derived from the independent measurements.

### 3.2.1 Comparison to AERONET AOD

For the comparison to the AOD from AERONET, we selected AOD values with time differences < 15 min and assigned them to the MAX-DOAS results. In the left figures of Fig. 12a and b, the relative frequencies of the individual sky conditions (indicated by the different colors) are shown for different intervals of the simultaneously measured AOD. Note that the sky conditions displayed between 0 and 100 % indicate the primary sky conditions, those displayed above 100 % indicate the secondary sky conditions. In the right figures of Fig. 12a and b, the corresponding absolute numbers of the different sky conditions are shown.

Figure 12 shows that the number of measurements classified as “clear sky with low aerosol load” decreases with increasing AERONET AOD. The highest fractions of “clear sky with high aerosol load” are found for AOD between 0.5 and 1.5. These findings are consistent with our expectations of these sky conditions.

## Cloud and aerosol classification for 2 1/2 years of MAX-DOAS observations

Y. Wang et al.

Title Page

Abstract

Introduction

Conclusions

References

Tables

Figures



Back

Close

Full Screen / Esc

Printer-friendly Version

Interactive Discussion



## Cloud and aerosol classification for 2 1/2 years of MAX-DOAS observations

Y. Wang et al.

Title Page

Abstract

Introduction

Conclusions

References

Tables

Figures

◀

▶

◀

▶

Back

Close

Full Screen / Esc

Printer-friendly Version

Interactive Discussion



For days with  $AOD < 1$ , if clouds are detected by MAX-DOAS, they are classified as either cloud holes or broken clouds. With increasing AOD the number of measurements classified as cloudy increase, and so does the fraction of continuous clouds and fog.

The two AERONET data sets show similar patterns, but level-1.0 data are more often classified as clouds than level-1.5 data, in accordance with the application of the AERONET cloud screening algorithm. As a consequence of cloud screening, the number of measurements is halved, and only a few points are left for the highest AOD bins.

### 3.2.2 Comparison to visibility meter

The comparison of the MAX-DOAS results with the visibility meter results is shown in Fig. 13. As expected the frequency of fog is highest for the lowest visibility. Also the frequency of “clear sky with high aerosol load” is highest for visibilities below 20 km. In contrast, the frequency of clear skies with low aerosol load is highest for the highest visibility values. The increasing fraction of continuous clouds and optically thick clouds with decreasing visibility might be caused by the occurrence of rain or possible factors which increase the probability of both aerosols and clouds (e.g. high humidity). The comparison of the MAX-DOAS results with the visibility meter confirms that the dependence of the visibility for the different sky conditions is well described by our classification scheme.

### 3.2.3 Comparison to aerosol and cloud data from OMI, GOME-2, and MODIS

In Figs. 14–17 the comparisons between the results from MAX-DOAS and the satellite instruments are shown. For these comparisons the MAX-DOAS results are averaged over one hour around the respective satellite overpass times (see Sects. 2.4.2 and 2.4.3 for spatial collocation criteria).

In Fig. 14a and b the MAX-DOAS results are compared with the AOD at 550 nm from MODIS on Aqua and on Terra, respectively. Similar distributions of the relative

## Cloud and aerosol classification for 2 1/2 years of MAX-DOAS observations

Y. Wang et al.

frequencies of the sky conditions along the AOD from MODIS are found for both of the MODIS instruments. Note that because some strict cloud screening and quality assurance controlling schemes are applied to the MODIS AOD data sets, most of the cloud contaminated data are discarded. The small number of measurements with AOD > 1.8 means that the relative frequencies of the sky conditions are probably not representative. The same is the case for the smallest AOD bin, although the reason for the small amount of measurements is probably that cases of AOD < 0.3 are rare in the investigated region. Except for these rarely encountered cases, the features of the distributions of the sky conditions along the AOD are quite similar with the comparison with AERONET AOD data sets. The relative frequencies of the sky condition of “clear with low aerosol” decrease along with the increasing AOD. Most of the sky conditions of “clear with high aerosol” occur in the AOD between 0.6 and 1.2. The fact that cloudy cases are still found, despite the rigorous cloud screening by MODIS, may be attributed to the difference in air masses sensed by MODIS and MAX-DOAS due to imperfect collocation. It may, however, also be caused by incorrect classification by the MAX-DOAS algorithm. Overall the results from MAX-DOAS are mostly consistent with the AOD data from MODIS.

In Fig. 15a–d the MAX-DOAS results are shown as functions of the effective CFs derived from OMI, GOME-2, and MODIS on Aqua and on Terra, respectively. The frequency of clear sky conditions (with either high or low aerosol load) is highest for small effective CFs. Two facts probably contribute to this finding. The first is the misclassification of aerosols as clouds by satellite instrument (see Sect. 3.2.4) and the second is the possibility of clouds being detected outside of the FOV of the MAX-DOAS instrument by satellite instrument (due to their different FOV and time difference of up to half hour), especially for MODIS due to its relative fine spatial resolution (CF and CP: 5 km × 5 km; COT: 1 km × 1 km). The frequencies of continuous clouds and optically thick clouds are highest for large effective CFs. Broken clouds are most frequent for the effective CF between 10 and 70 %. Compared with other satellites, a higher frequency of fog is found for GOME-2, which can be explained by the higher probability for fog at the earlier over-

Title Page

Abstract

Introduction

Conclusions

References

Tables

Figures

◀

▶

◀

▶

Back

Close

Full Screen / Esc

Printer-friendly Version

Interactive Discussion



## Cloud and aerosol classification for 2 1/2 years of MAX-DOAS observations

Y. Wang et al.

Title Page

Abstract

Introduction

Conclusions

References

Tables

Figures

◀

▶

◀

▶

Back

Close

Full Screen / Esc

Printer-friendly Version

Interactive Discussion



pass time of GOME-2 (09:30 LT) compared to OMI (13:30 LT). The similar, but smaller, difference for fog is found between MODIS on Aqua (overpass time: 13:30 LT) and on Terra (overpass time: 10:30 LT). The sky condition of “continuous clouds (small SZA)” rarely occurs for GOME-2 due to its early overpass time, because this sky condition occurs only for small SZA. From all comparisons shown in Fig. 15 we conclude that the cloudy sky conditions derived from MAX-DOAS observations are related to effective CF derived from satellite.

In Fig. 16 the MAX-DOAS results are compared to the COT derived from MODIS. For this comparison we used only MODIS data with geometrical CF > 80 %. Clear sky conditions (with low and high aerosol load) are only found for cases with small COT, which can be interpreted by the same two facts as the comparison with effective CFs. Cases of broken clouds and cloud holes are mainly found for small COT, continuous clouds for medium COT, and optically thick clouds for large COT, in agreement with our expectations. Slightly different dependencies are found for both MODIS instruments, especially with respect to the fractions of optically thick clouds and continuous clouds. However, the differences between MODIS instruments are probably not significant in view of the number of data points.

In Fig. 17 the MAX-DOAS results are shown as function of the cloud pressure derived from OMI, GOME-2 and both MODIS instruments. For the comparison, we used the criteria of effective CF above 20 % to filter the cloud pressure data from different satellites because the CP cannot be accurately retrieved for few clouds in the satellite view (Weisz et al., 2007; Wang et al., 2008). Similar distributions of the relative frequency of the sky conditions along the cloud pressure are found for all four cases. Continuous clouds have the highest probability for medium cloud pressures, which is probably related to the typical altitudes of stratus clouds. Compared to continuous clouds, broken clouds have larger cloud top pressure, which probably indicates that most of broken clouds belong to cumulus. The category of cloud holes occurs mostly equally in various cloud top pressures. Also fog is usually assigned to high cloud pressures representing fog events at low altitude (some of them might of course be overlaid

by higher clouds). And a much higher frequency of fog is found by GOME-2 compared to other instruments probably due to its earlier overpass time (09:30 LT). Much fewer absolute numbers of the observed sky conditions are assigned to small CP from OMI and GOME-2 than that from MODIS, which is well explained by the general overestimation of CP by OMI and GOME-2 (see the Supplement). Although no clear relationship between the MAX-DOAS results and the satellite cloud pressure can be expected, the findings show that both high and low clouds can be detected using the MAX-DOAS classification scheme.

### 3.2.4 Cloud properties retrieved from satellite observations for clear sky cases identified by MAX-DOAS

As discussed in the previous section, for part of the clear sky cases (classified from MAX-DOAS observations) the corresponding satellite observations indicate the presence of clouds. There are three possible reasons for this: (1) the satellite instruments wrongly attribute strong aerosol scattering to clouds, (2) the MAX-DOAS classification mistakes clouds for aerosols, (3) the instruments sense different air masses (due to imperfect collocation), and hence different sky conditions. In this section we investigate the sensitivity of the satellite cloud products to the sky condition derived from our cloud classification scheme. We only consider clear sky conditions (with low or high aerosol load). The respective cloud properties derived from the satellite observations are presented in Fig. 18. The satellite cloud products are systematically different for cases with either low or high aerosol load: the mean geometrical and effective CFs derived from the four instruments are appreciably larger for cases with high aerosol load than for low aerosol load. This may be an indication that the cloud parameters derived from satellite are indeed sensitive to the presence and amount of aerosols. For MODIS, Brennan et al. (2005) concludes that the aerosol contamination of MODIS collection 04 cloud products occurs when aerosol optical depth is larger than 0.6. Although the improved collection 05 cloud products, used in this study, apply an improved cloud masking technique, our finding indicates that the aerosol contamination of MODIS cloud products

## Cloud and aerosol classification for 2 1/2 years of MAX-DOAS observations

Y. Wang et al.

Title Page

Abstract

Introduction

Conclusions

References

Tables

Figures

◀

▶

◀

▶

Back

Close

Full Screen / Esc

Printer-friendly Version

Interactive Discussion





## Cloud and aerosol classification for 2 1/2 years of MAX-DOAS observations

Y. Wang et al.

- a. We developed a simple method for the quantification and correction for the effects of possible instrument degradation.
- b. Due to the mismatch of measured and simulated radiances for  $SZA < 40^\circ$ , we developed a way to extract reference values mostly from measurements.
- 5 c. Optically thick clouds were identified only based on the measured radiances because of the challenge of the absolute calibration of the  $O_4$  retrieval for the long measurement time series.
- d. We extended the cloud classification scheme by using different criteria for large or small SZA for the determination of continuous clouds. This modification will be especially important for measurements during summer at latitudes between  $\pm 60^\circ$ .
- 10 e. We added a category named “extremely high midday CI”, which describes very rare cases with strongly reduced radiance in the blue spectral range compared to the UV.

We compared the results of our MAX-DOAS cloud classification scheme with several independent data sets: AOD from AERONET and MODIS, visibility derived from visibility meters, as well as effective cloud fractions, cloud top pressures and cloud optical thickness derived from different satellite instruments (MODIS, OMI, GOME-2). These statistical analyses overall confirmed the validity of our classification scheme. For example, most cases of clear sky conditions with low or high aerosol load were correctly assigned to the respective AOD derived from AERONET and MODIS. Also the dependence of the cloud classification results on cloud optical thickness and effective cloud fraction derived from satellite was well represented.

The dependence of the results of the MAX-DOAS cloud classification scheme on the cloud optical thickness motivated us to further investigate the general ability of the scheme to identify optically thin clouds. For MODIS observations of thick clouds ( $COT > 10$ ), the sky conditions derived from MAX-DOAS comprise mostly optically thick clouds, continuous clouds and fog. For MODIS observations of thin clouds ( $COT < 10$ ), the sky

Title Page

Abstract

Introduction

Conclusions

References

Tables

Figures

◀

▶

◀

▶

Back

Close

Full Screen / Esc

Printer-friendly Version

Interactive Discussion





National Natural Science Foundation of China (grant no.: 41275038).

The article processing charges for this open-access publication were covered by the Max Planck Society.

## 5 References

- Acarreta, J. R., De Haan, J. F., and Stammes, P.: Cloud pressure retrieval using the O<sub>2</sub>–O<sub>2</sub> absorption band at 477 nm, *J. Geophys. Res.*, 109, D05204, doi:10.1029/2003JD003915, 2004.
- Baum, B. A. and Platnick, S.: Introduction to MODIS cloud products, in: *Earth Science Satellite Remote Sensing*, Springer, Berlin Heidelberg, 74–91, 2006.
- Bobrowski, N., Honninger, G., Galle, B., and Platt, U.: Detection of bromine monoxide in a volcanic plume, *Nature*, 423, 273–276, 2003.
- Boersma, K. F., Eskes, H. J., and Brinksma, E. J.: Error analysis for tropospheric NO<sub>2</sub> retrieval from space, *J. Geophys. Res.*, 109, D04311, doi:10.1029/2003JD003962, 2004.
- 15 Boersma, K. F., Eskes, H. J., Veefkind, J. P., Brinksma, E. J., van der A, R. J., Sneep, M., van den Oord, G. H. J., Levelt, P. F., Stammes, P., Gleason, J. F., and Bucsela, E. J.: Near-real time retrieval of tropospheric NO<sub>2</sub> from OMI, *Atmos. Chem. Phys.*, 7, 2103–2118, doi:10.5194/acp-7-2103-2007, 2007.
- 20 Bogumil, K., Orphal, J., Homann, T., Voigt, S., Spietz, P., Fleischmann, O. C., Vogel, A., Hartmann, M., Kromminga, H., Bovensmann, H., Frerick, J., and Burrows, J. P.: Measurements of molecular absorption spectra with the SCIAMACHY pre-flight model: instrument characterization and reference data for atmospheric remote-sensing in the 230–2380 nm region, *J. Photoch. Photobio. A*, 157, 167–184, 2003.
- Bohn, B., Rohrer, F., Brauers, T., and Wahner, A.: Actinometric measurements of NO<sub>2</sub> photolysis frequencies in the atmosphere simulation chamber SAPHIR, *Atmos. Chem. Phys.*, 5, 493–503, doi:10.5194/acp-5-493-2005, 2005.
- 25 Brennan, J. I., Kaufman, Y. J., Koren, I., and Li, R. R.: Aerosol-cloud interaction-misclassification of MODIS clouds in heavy aerosol, *Geosci. Remote Sens.*, 43, 911–915, doi:10.1109/TGRS.2005.844662, 2005.

## Cloud and aerosol classification for 2 1/2 years of MAX-DOAS observations

Y. Wang et al.

Title Page

Abstract

Introduction

Conclusions

References

Tables

Figures

◀

▶

◀

▶

Back

Close

Full Screen / Esc

Printer-friendly Version

Interactive Discussion



## Cloud and aerosol classification for 2 1/2 years of MAX-DOAS observations

Y. Wang et al.

Title Page

Abstract

Introduction

Conclusions

References

Tables

Figures

◀

▶

◀

▶

Back

Close

Full Screen / Esc

Printer-friendly Version

Interactive Discussion

- Brinksma, E. J., Pinardi, G., Volten, H., Braak, R., Richter, A., Schönhardt, A., van Roozendael, M., Fayt, C., Hermans, C., Dirksen, R. J., Vlemmix, T., Berkhout, A. J. C., Swart, D. P. J., Oetjen, H., Wittrock, F., Wagner, T., Ibrahim, O. W., de Leeuw, G., Moerman, M., Curier, R. L., Celarier, E. A., Cede, A., Knap, W. H., Veefkind, J. P., Eskes, H. J., Allaart, M., Rothe, R., Pipers, A. J. M., and Levelt, P. F.: The 2005 and 2006 DANDELIONS NO<sub>2</sub> and aerosol inter-comparison campaigns, *J. Geophys. Res.*, 113, D16S46, doi:10.1029/2007JD008808, 2008.
- Callies, J., Corpaccioli, E., Eisinger, M., Hahne, A., and Lefebvre, A.: GOME-2 – MetOp’s Second Generation Sensor for Operational Ozone Monitoring, *ESA Bulletin*, No. 102, 2000.
- Chimot, J., Veefkind, J. P., Vlemmix, T., and Levelt, P. F.: Analysis of the aerosol effects on the current NO<sub>2</sub> and cloud retrievals from the OMI satellite instrument, EOS Aura Science Team Meeting 10th year anniversary celebration, College Park, MD, USA, 15 September 2014, doi:10.13140/2.1.2874.0169, 2015.
- Clémer, K., Fayt, C., Hendrick, F., Hermans, C., Pinardi, G., and Van Roozendael, M.: The simultaneous retrieval of tropospheric aerosol extinction and NO<sub>2</sub> vertical profiles from MAX-DOAS measurements in Beijing, in: *Proceedings of the 8th International Symposium on Tropospheric Profiling*, ISBN 978-90-6960-233-2, Delft, the Netherlands, 19–23 October 2009, 10, 2009.
- Clémer, K., Van Roozendael, M., Fayt, C., Hendrick, F., Hermans, C., Pinardi, G., Spurr, R., Wang, P., and De Mazière, M.: Multiple wavelength retrieval of tropospheric aerosol optical properties from MAXDOAS measurements in Beijing, *Atmos. Meas. Tech.*, 3, 863–878, doi:10.5194/amt-3-863-2010, 2010.
- DeMore, W. B., Sander, S. P., Golden, D. M., Hampson, R. F., Kurylo, M. J., Howard, C. J., Ravishankara, A. R., Kolb, C. E., and Molina, M. J.: *Chemical Kinetics and Photochemical Data for Use in Stratospheric Modeling*, Evaluation No. 12, JPL Publication 97-4, 1997.
- Deutschmann, T.: *Atmospheric Radiative Transfer Modelling with Monte Carlo Methods*, Ms thesis, University Heidelberg, Germany, 2009.
- Erle, F., Pfeilsticker, K., and Platt, U.: On the influence of tropospheric clouds on zenith scattered light measurements of stratospheric species, *Geophys. Res. Lett.*, 22, 2725–2728, 1995.
- Hermans, C., Pinardi, G., and Van Roozendael, M.: The simultaneous retrieval of tropospheric aerosol extinction and NO<sub>2</sub> vertical profiles from MAXDOAS measurements in Beijing, in: *Proceedings of the 8th International Symposium on Tropospheric Profiling*, ISBN 978-90-6960-233-2, Delft, the Netherlands, 19–23 October 2009, 10, 2009.

## Cloud and aerosol classification for 2 1/2 years of MAX-DOAS observations

Y. Wang et al.

Title Page

Abstract

Introduction

Conclusions

References

Tables

Figures

◀

▶

◀

▶

Back

Close

Full Screen / Esc

Printer-friendly Version

Interactive Discussion



- Henyey, L. G. and Greenstein, J. L.: Diffuse radiation in the galaxy, *Astrophys. J.*, 93, 70–83, 1941.
- Hofzumahaus, A., Kraus, A., and Müller, M.: Solar actinic flux spectroradiometry: a technique for measuring photolysis frequencies in the atmosphere, *Appl. Optics*, 38, 4443–4460, 1999.
- 5 Erie, F., Pfeilsticker, K., and Platt, U.: On the influence of tropospheric clouds on zenith-scattered-light measurements of stratospheric species, *Geophys. Res. Lett.*, 22, 2725, doi:10.1029/95GL02789, 1995.
- Fayt, C. and van Roozendaal, M.: WinDOAS 2.1 Software User Manual, IASB/BIRA, available at: <http://bro.aeronomie.be/WinDOAS-SUM-210b.pdf> (last access: 29 April 2015), 2009.
- 10 Frieß, U., Monks, P. S., Remedios, J. J., Rozanov, A., Sinreich, R., Wagner, T., and Platt, U.: MAX-DOAS O<sub>4</sub> measurements: a new technique to derive information on atmospheric aerosols: 2. Modeling studies, *J. Geophys. Res.*, 111, D14203, doi:10.1029/2004JD004904, 2006.
- Frieß, U., Sihler, H., and Sander, R.: The vertical distribution of BrO and aerosols in the Arctic: measurements by active and passive differential optical absorption spectroscopy, *J. Geophys. Res.*, 116, D00R04, doi:10.1029/2011JD015938, 2011.
- 15 Greenblatt, G. D., Orlando, J. J., Burkholder, J. B., and Ravishankara, A. R.: Absorption measurements of oxygen between 330 and 1140 nm, *J. Geophys. Res.*, 95, 18577–18582, 1990.
- Gielen, C., Van Roozendaal, M., Hendrick, F., Pinardi, G., Vlemmix, T., De Bock, V., De Backer, H., Fayt, C., Hermans, C., Gillotay, D., and Wang, P.: A simple and versatile cloud-screening method for MAX-DOAS retrievals, *Atmos. Meas. Tech.*, 7, 3509–3527, doi:10.5194/amt-7-3509-2014, 2014.
- 20 Grainger, J. F. and Ring, J.: Anomalous Fraunhofer line profiles, *Nature*, 193, p. 762, doi:10.1038/193762a0, 1962.
- 25 Holben, B. N., Eck, T. F., Slutsker, I., Tanre, D., Buis, J. P., Setzer, A., Vermote, E., Reagan, J. A., Kaufman, Y., Nakajima, T., Lavenu, F., Jankowiak, I., and Smirnov, A.: AERONET – a federated instrument network and data archive for aerosol characterization, *Remote Sens. Environ.*, 66, 1–16, 1998.
- 30 Holben, B. N., Tanre, D., Smirnov, A., Eck, T. F., Slutsker, I., Abuhassan, N., Newcomb, W. W., Schafer, J., Chatenet, B., Lavenu, F., Kaufman, Y. J., Van de Castle, J., Setzer, A., Markham, B., Clark, D., Frouin, R., Halthore, R., Karnieli, A., O'Neill, N. T., Pietras, C., Pinker, R. T., Voss, K., and Zibordi, Z.: An emerging ground-based aerosol climatology: aerosol optical depth from AERONET, *J. Geophys. Res.*, 106, 12067–12097, 2001.

**Cloud and aerosol  
classification for 2  
1/2 years of  
MAX-DOAS  
observations**

Y. Wang et al.

Title Page

Abstract

Introduction

Conclusions

References

Tables

Figures

◀

▶

◀

▶

Back

Close

Full Screen / Esc

Printer-friendly Version

Interactive Discussion



Hönninger, G., von Friedeburg, C., and Platt, U.: Multi axis differential optical absorption spectroscopy (MAX-DOAS), *Atmos. Chem. Phys.*, 4, 231–254, doi:10.5194/acp-4-231-2004, 2004.

Heckel, A., Richter, A., Tarsu, T., Wittrock, F., Hak, C., Pundt, I., Junkermann, W., and Burrows, J. P.: MAX-DOAS measurements of formaldehyde in the Po-Valley, *Atmos. Chem. Phys.*, 5, 909–918, doi:10.5194/acp-5-909-2005, 2005.

Irie, H., Kanaya, Y., Akimoto, H., Iwabuchi, H., Shimizu, A., and Aoki, K.: First retrieval of tropospheric aerosol profiles using MAX-DOAS and comparison with lidar and sky radiometer measurements, *Atmos. Chem. Phys.*, 8, 341–350, doi:10.5194/acp-8-341-2008, 2008.

Irie, H., Takashima, H., Kanaya, Y., Boersma, K. F., Gast, L., Wittrock, F., Brunner, D., Zhou, Y., and Van Roozendaal, M.: Eight-component retrievals from ground-based MAX-DOAS observations, *Atmos. Meas. Tech.*, 4, 1027–1044, doi:10.5194/amt-4-1027-2011, 2011.

Kaufman, Y. J., Tanré, D., and Boucher, O.: A satellite view of aerosols in the climate system, *Nature*, 419, 215–223, 2002.

King, M. D., Tsay, S.-C., Platnick, S. E., Wang, M., and Liou, K.-N.: Cloud retrieval algorithms for MODIS: optical thickness, effective particle radius, and thermodynamic phase, *Tech. Rep. ATBD-MOD-05*, NASA, Washington, D.C., 1998.

King, M. D., Platnick, S., Yang, P., Arnold, G. T., Gray, M. A., Riédi, J. C., Ackerman, S. A., Liou, K. N.: Remote sensing of liquid water and ice cloud optical thickness, and effective radius in the arctic: application of airborne multispectral MAS data, *J. Atmos. Ocean. Tech.*, 21, 857–875, 2004.

Kraus, S.: DOASIS, a Framework Design for DOAS, Ph.D. thesis, University of Mannheim, available at: [http://hci.iwr.uni-heidelberg.de/publications/dip/2006/Kraus\\_PhD2006.pdf](http://hci.iwr.uni-heidelberg.de/publications/dip/2006/Kraus_PhD2006.pdf), 2006.

Levelt, P. F., Hilsenrath, E., Leppelmeier, G. W., van den Oord, G. H. J., Bhartia, P. K., Tamminen, J., de Haan, J. F., and Veefkind, J. P.: Science objectives of the ozone monitoring instrument, *IEEE T. Geosci. Remote*, 44, 1199–1208, doi:10.1109/TGRS.2006.872336, 2006a.

Levelt, P. F., van den Oord, G. H. J., Dobber, M. R., Malkki, A., Visser, H., de Vries, J., Stammes, P., Lundell, J., and Saari, H.: The Ozone Monitoring Instrument, *IEEE T. Geosci. Remote*, 44, 1093–1101, doi:10.1109/TGRS.2006.872333, 2006b.

Levy, R. C., Remer, L. A., Kleidman, R. G., Mattoo, S., Ichoku, C., Kahn, R., and Eck, T. F.: Global evaluation of the Collection 5 MODIS dark-target aerosol products over land, *Atmos. Chem. Phys.*, 10, 10399–10420, doi:10.5194/acp-10-10399-2010, 2010.

## Cloud and aerosol classification for 2 1/2 years of MAX-DOAS observations

Y. Wang et al.

Title Page

Abstract

Introduction

Conclusions

References

Tables

Figures

◀

▶

◀

▶

Back

Close

Full Screen / Esc

Printer-friendly Version

Interactive Discussion



- Li, A., Xie, P. H., Liu, C., Liu, J. G., and Liu, W. Q.: A scanning multi-Axis differential optical absorption spectroscopy system for measurement of tropospheric NO<sub>2</sub> in Beijing, Chin. Phys. Lett., 24, 2859–2862, doi:10.1088/0256-307X/24/10/041, 2007.
- Li, X., Brauers, T., Shao, M., Garland, R. M., Wagner, T., Deutschmann, T., and Wahner, A.: MAX-DOAS measurements in southern China: retrieval of aerosol extinctions and validation using ground-based in-situ data, Atmos. Chem. Phys., 10, 2079–2089, doi:10.5194/acp-10-2079-2010, 2010.
- Li, X., Brauers, T., Hofzumahaus, A., Lu, K., Li, Y. P., Shao, M., Wagner, T., and Wahner, A.: MAX-DOAS measurements of NO<sub>2</sub>, HCHO and CHOCHO at a rural site in Southern China, Atmos. Chem. Phys., 13, 2133–2151, doi:10.5194/acp-13-2133-2013, 2013.
- Munro, R., Eisinger, M., Anderson, C., Callies, J., Corpaccioli, E., Lang, R., Lefebvre, A., Livschitz, Y., and Albinana, A. P.: GOME-2 on MetOp, Proc. of The 2006 EUMETSAT Meteorological Satellite Conference, Helsinki, Finland, 12–16 June 2006, EUMETSAT p. 48, 2006.
- Ma, J. Z., Beirle, S., Jin, J. L., Shaiganfar, R., Yan, P., and Wagner, T.: Tropospheric NO<sub>2</sub> vertical column densities over Beijing: results of the first three years of ground-based MAX-DOAS measurements (2008–2011) and satellite validation, Atmos. Chem. Phys., 13, 1547–1567, doi:10.5194/acp-13-1547-2013, 2013.
- Nebuloni, R.: Empirical relationships between extinction co-efficient and visibility in fog, Appl. Optics, 44, 3795–3804, doi:10.1364/AO.44.003795, 2005.
- Pikelnaya, O., Hurlock, S. C., Trick, S., and Stutz, J.: Intercomparison of multi-axis and long-path optical absorption spectroscopy measurements in the marine boundary layer, J. Geophys. Res., 112, D10S01, doi:10.1029/2006JD007727, 2007.
- Peters, A. J. M., Boersma, K. F., Kroon, M., Hains, J. C., Van Roozendael, M., Wittrock, F., Abuhassan, N., Adams, C., Akrami, M., Allaart, M. A. F., Apituley, A., Beirle, S., Bergwerff, J. B., Berkhout, A. J. C., Brunner, D., Cede, A., Chong, J., Clémer, K., Fayt, C., Frieß, U., Gast, L. F. L., Gil-Ojeda, M., Goutail, F., Graves, R., Griesfeller, A., Großmann, K., Hemerijckx, G., Hendrick, F., Henzing, B., Herman, J., Hermans, C., Hoexum, M., van der Hoff, G. R., Irie, H., Johnston, P. V., Kanaya, Y., Kim, Y. J., Klein Baltink, H., Kreher, K., de Leeuw, G., Leigh, R., Merlaud, A., Moerman, M. M., Monks, P. S., Mount, G. H., Navarro-Comas, M., Oetjen, H., Pazmino, A., Perez-Camacho, M., Peters, E., du Piesanie, A., Pinardi, G., Puentedura, O., Richter, A., Roscoe, H. K., Schönhardt, A., Schwarzenbach, B., Shaiganfar, R., Sluis, W., Spinei, E., Stolk, A. P., Strong, K., Swart, D. P. J., Takashima, H., Vlemmix, T., Vrekoussis, M., Wagner, T., Whyte, C., Wilson, K. M., Yela, M., Yilmaz, S., Zieger, P.,



**Cloud and aerosol  
classification for 2  
1/2 years of  
MAX-DOAS  
observations**

Y. Wang et al.

Title Page

Abstract

Introduction

Conclusions

References

Tables

Figures

◀

▶

◀

▶

Back

Close

Full Screen / Esc

Printer-friendly Version

Interactive Discussion



Takashima, H., Irie, H., Kanaya, Y., Shimizu, A., Aoki, K., and Akimoto, H.: Atmospheric aerosol variations at Okinawa Island in Japan observed by MAX-DOAS using a new cloud-screening method, *J. Geophys. Res.*, 114, D18213, doi:10.1029/2009JD011939, 2009.

5 Theys, N., Van Roozendael, M., Hendrick, F., Fayt, C., Hermans, C., Baray, J.-L., Goutail, F., Pommereau, J.-P., and De Mazière, M.: Retrieval of stratospheric and tropospheric BrO columns from multi-axis DOAS measurements at Reunion Island (21° S, 56° E), *Atmos. Chem. Phys.*, 7, 4733–4749, doi:10.5194/acp-7-4733-2007, 2007.

10 Vandaele, A. C., Hermans, C., Simon, P. C., Carleer, M., Colin, R., Fally, S., Mérienne, M.-F., Jenouvrier, A., and Coquart, B.: Measurements of the NO<sub>2</sub> absorption cross section from 42000 cm<sup>-1</sup> to 10000 cm<sup>-1</sup> (238–1000 nm) at 220 K and 294 K, *J. Quant. Spectrosc. Ra.*, 59, 171–184, 1998.

Vlemmix, T., Piters, A. J. M., Stammes, P., Wang, P., and Levelt, P. F.: Retrieval of tropospheric NO<sub>2</sub> using the MAX-DOAS method combined with relative intensity measurements for aerosol correction, *Atmos. Meas. Tech.*, 3, 1287–1305, doi:10.5194/amt-3-1287-2010, 2010.

15 Vlemmix, T., Piters, A. J. M., Berkhout, A. J. C., Gast, L. F. L., Wang, P., and Levelt, P. F.: Ability of the MAX-DOAS method to derive profile information for NO<sub>2</sub>: can the boundary layer and free troposphere be separated?, *Atmos. Meas. Tech.*, 4, 2659–2684, doi:10.5194/amt-4-2659-2011, 2011.

20 Vlemmix, T., Hendrick, F., Pinardi, G., De Smedt, I., Fayt, C., Hermans, C., Piters, A., Wang, P., Levelt, P., and Van Roozendael, M.: MAX-DOAS observations of aerosols, formaldehyde and nitrogen dioxide in the Beijing area: comparison of two profile retrieval approaches, *Atmos. Meas. Tech.*, 8, 941–963, doi:10.5194/amt-8-941-2015, 2015.

25 Wielicki, B. A. and Coakley Jr., J. A.: Cloud retrieval using infrared sounder data: error analysis, *J. Appl. Meteorol.*, 20, 157–169, 1981.

Wittrock, F., Oetjen, H., Richter, A., Fietkau, S., Medeke, T., Rozanov, A., and Burrows, J. P.: MAX-DOAS measurements of atmospheric trace gases in Ny-Ålesund – Radiative transfer studies and their application, *Atmos. Chem. Phys.*, 4, 955–966, doi:10.5194/acp-4-955-2004, 2004.

30 Wagner, T., Erie, F., Marquard, L., Otten, C., Pfeilsticker, K., Senne, T., Stutz, J., and Platt, U.: Cloudy sky optical paths as derived from differential optical absorption spectroscopy observations, *J. Geophys. Res.*, 103, 25307, doi:10.1029/98JD01021, 1998.

## Cloud and aerosol classification for 2 1/2 years of MAX-DOAS observations

Y. Wang et al.

Title Page

Abstract

Introduction

Conclusions

References

Tables

Figures

◀

▶

◀

▶

Back

Close

Full Screen / Esc

Printer-friendly Version

Interactive Discussion



- Wagner, T., von Friedeburg, C., Wenig, M., Otten, C., and Platt, U.: UV/vis observations of atmospheric  $O_4$  absorptions using direct moon light and zenith scattered sunlight under clear and cloudy sky conditions, *J. Geophys. Res.*, 107, D204424, doi:10.1029/2001JD001026, 2002.
- 5 Wagner, T., Dix, B., von Friedeburg, C., Frieß, U., Sanghavi, S., Sinreich, R., and Platt, U.: MAX-DOAS  $O_4$  measurements: a new technique to derive information on atmospheric aerosols – Principles and information content, *J. Geophys. Res.*, 109, D22205, doi:10.1029/1999GL900243, 2004.
- Wagner, T., Beirle, S., and Deutschmann, T.: Three-dimensional simulation of the Ring effect in observations of scattered sun light using Monte Carlo radiative transfer models, *Atmos. Meas. Tech.*, 2, 113–124, doi:10.5194/amt-2-113-2009, 2009.
- 10 Wagner, T., Beirle, S., Brauers, T., Deutschmann, T., Frieß, U., Hak, C., Halla, J. D., Heue, K. P., Junkermann, W., Li, X., Platt, U., and Pundt-Gruber, I.: Inversion of tropospheric profiles of aerosol extinction and HCHO and  $NO_2$  mixing ratios from MAX-DOAS observations in Milano during the summer of 2003 and comparison with independent data sets, *Atmos. Meas. Tech.*, 4, 2685–2715, doi:10.5194/amt-4-2685-2011, 2011.
- 15 Wagner, T., Apituley, A., Beirle, S., Dörner, S., Friess, U., Remmers, J., and Shaiganfar, R.: Cloud detection and classification based on MAX-DOAS observations, *Atmos. Meas. Tech.*, 7, 1289–1320, doi:10.5194/amt-7-1289-2014, 2014.
- 20 Wang, P., Stammes, P., van der A, R., Pinardi, G., and van Roozendaal, M.: FRESCO+: an improved  $O_2$  A-band cloud retrieval algorithm for tropospheric trace gas retrievals, *Atmos. Chem. Phys.*, 8, 6565–6576, doi:10.5194/acp-8-6565-2008, 2008.
- Wang, P., Tuinder, O. N. E., Tilstra, L. G., de Graaf, M., and Stammes, P.: Interpretation of FRESCO cloud retrievals in case of absorbing aerosol events, *Atmos. Chem. Phys.*, 12, 9057–9077, doi:10.5194/acp-12-9057-2012, 2012.
- 25 Wang, P. and Stammes, P.: Evaluation of SCIAMACHY Oxygen A band cloud heights using Cloudnet measurements, *Atmos. Meas. Tech.*, 7, 1331–1350, doi:10.5194/amt-7-1331-2014, 2014.
- Winterrath, T., Koroso, T. P., Richter, A., and Burrows, J. P.: Enhanced  $O_3$  and  $NO_2$  in thunderstorm clouds: convection or production, *Geophys. Res. Lett.*, 26, 1291, doi:10.1029/2007GL030676, 1999.
- 30

Weisz, E., Li, J., Menzel, W. P., Heidinger, A. K., Kahn, B. H., and Liu, C. Y.: Comparison of AIRS, MODIS, CloudSat and CALIPSO cloud top height retrievals, *Geophys. Res. Lett.*, 34, L17811, doi:10.1029/2007GL030676, 2007.

5 Zhao, W. J., Zhang, N., and Sun, J. N.: Spatiotemporal variations of cloud amount over the Yangtze River Delta, China, *J. Meteorol. Res.*, 28, 371–380, 2014.

# AMTD

8, 4653–4709, 2015

## Cloud and aerosol classification for 2 1/2 years of MAX-DOAS observations

Y. Wang et al.

Title Page

Abstract

Introduction

Conclusions

References

Tables

Figures



Back

Close

Full Screen / Esc

Printer-friendly Version

Interactive Discussion



## Cloud and aerosol classification for 2 1/2 years of MAX-DOAS observations

Y. Wang et al.

**Table 1.** Quantities derived from MAX-DOAS observations for cloud classification, their abbreviations and thresholds.

Quantity for cloud classification	Abbreviation	Threshold	Threshold (Wagner et al., 2014)
Normalized CI (340 nm/420 nm) for zenith view	$CI_z^n$	0.84	0.65
Normalized temporal smoothness indicator of CI for zenith view	$TSI_z^n$	$8 \times 10^{-8} \text{ s}^{-2}$	$1.2 \times 10^{-7} \text{ s}^{-2}$
Sum of normalized temporal smoothness indicator of CI for non-zenith view	$TSI_L^n$	$2.5 \times 10^{-7} \text{ s}^{-2}$	$3.3 \times 10^{-7} \text{ s}^{-2}$
Spread of the CI	$Sp_{CI}$	0.3	0.14
Normalized radiance at 380 nm	$Ra_z^n$	0.94	0.9
Spread of the O <sub>4</sub> dAMF	$Sp_{O_4}$	0.4	0.4

Title Page

Abstract

Introduction

Conclusions

References

Tables

Figures

◀

▶

◀

▶

Back

Close

Full Screen / Esc

Printer-friendly Version

Interactive Discussion

## Cloud and aerosol classification for 2 1/2 years of MAX-DOAS observations

Y. Wang et al.

[Title Page](#)
[Abstract](#)
[Introduction](#)
[Conclusions](#)
[References](#)
[Tables](#)
[Figures](#)
[◀](#)
[▶](#)
[◀](#)
[▶](#)
[Back](#)
[Close](#)
[Full Screen / Esc](#)
[Printer-friendly Version](#)
[Interactive Discussion](#)

**Table 2.** Conditions used for the cloud classification scheme for MAX-DOAS observations at Wuxi.

Sky condition	Determination criteria	Determination criteria (Wagner et al., 2014)
Clear with low aerosol	high $CI_z^n$ & low $TSI_z^n$ & low $TSI_L^n$ & high $Sp_{CI}$	high $CI_z^n$ & low $TSI_z^n$
Extremely high midday CI	$CI_z^n$ larger than 1.3 & high $Sp_{CI}$ & low $Ra_z^n$	none
Clear with high aerosol	low $CI_z^n$ & low $TSI_z^n$ & low $TSI_L^n$ & high $Sp_{CI}$	low $CI_z^n$ & low $TSI_z^n$ & high $Sp_{CI}$
Cloud holes (zenith)	high $CI_z^n$ & high $TSI_z^n$	high $CI_z^n$ & high $TSI_z^n$
Cloud holes (low elevation)	high $CI_z^n$ & low $TSI_z^n$ & high $TSI_L^n$	high $CI_z^n$ & high $TSI_L^n$
Broken clouds	low $CI_z^n$ & high $TSI_z^n$ or high $TSI_L^n$	low $CI_z^n$ & high $TSI_z^n$
Continuous clouds (large SZA)	low $CI_z^n$ & low $TSI_z^n$ & low $TSI_L^n$ & low $Sp_{CI}$	low $CI_z^n$ & low $TSI_z^n$ & low $Sp_{CI}$
Continuous clouds (small SZA)	high $CI_z^n$ & low $TSI_z^n$ & low $TSI_L^n$ & low $Sp_{CI}$	none
Fog	low $CI_z^n$ & low $Sp_{O_4}$	low $CI_z^n$ & low $Sp_{O_4}$
Optically thick clouds	(low $CI_z^n$ or continuous clouds for small SZA) & low $Ra_z^n$	low $CI_z^n$ & low $Ra_z^n$ or high $O_4$ AMF

## Cloud and aerosol classification for 2 1/2 years of MAX-DOAS observations

Y. Wang et al.

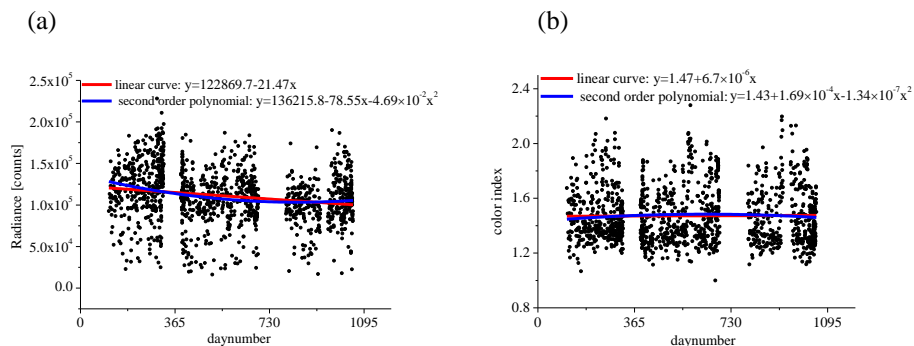


**Figure 1.** The radiance at 380 nm **(a)** and the color index (340 nm/420 nm) **(b)** derived from MAX-DOAS observations in zenith view against the daynumber (the daynumber of one corresponds to 1 January 2011) for an SZA interval of 49–51°. The red and blue curves represent a linear fitted slope and second order polynomial as functions of the daynumber, respectively.

Title Page

Abstract

Introduction

Conclusions

References

Tables

Figures

◀

▶

◀

▶

Back

Close

Full Screen / Esc

Printer-friendly Version

Interactive Discussion



**Cloud and aerosol  
classification for 2  
1/2 years of  
MAX-DOAS  
observations**

Y. Wang et al.

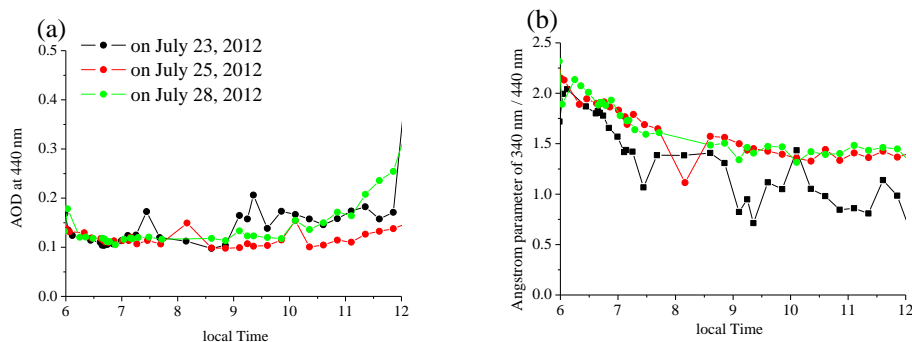


**Figure 2.** Time series of the AOD at 440 nm **(a)** and the Angström parameter of 340 nm against 440 nm **(b)** from AERONET on 23, 25 and 28 July 2012.

Title Page

Abstract

Introduction

Conclusions

References

Tables

Figures

◀

▶

◀

▶

Back

Close

Full Screen / Esc

Printer-friendly Version

Interactive Discussion



## Cloud and aerosol classification for 2 1/2 years of MAX-DOAS observations

Y. Wang et al.

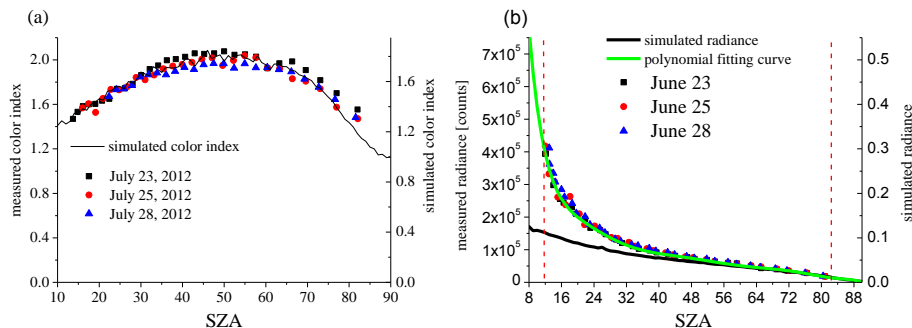


**Figure 3.** The comparisons of measurements of **(a)** the color index (340 nm/420 nm), and **(b)** the radiance at 380 nm for three clear half days with their corresponding values derived from radiative transfer simulations (black lines). In subfigure **(b)** the green line indicates the polynomial fit of the measured radiance on the three half days; the red dashed lines indicate the SZA of 12 and 82°.

Title Page

Abstract

Introduction

Conclusions

References

Tables

Figures

◀

▶

◀

▶

Back

Close

Full Screen / Esc

Printer-friendly Version

Interactive Discussion



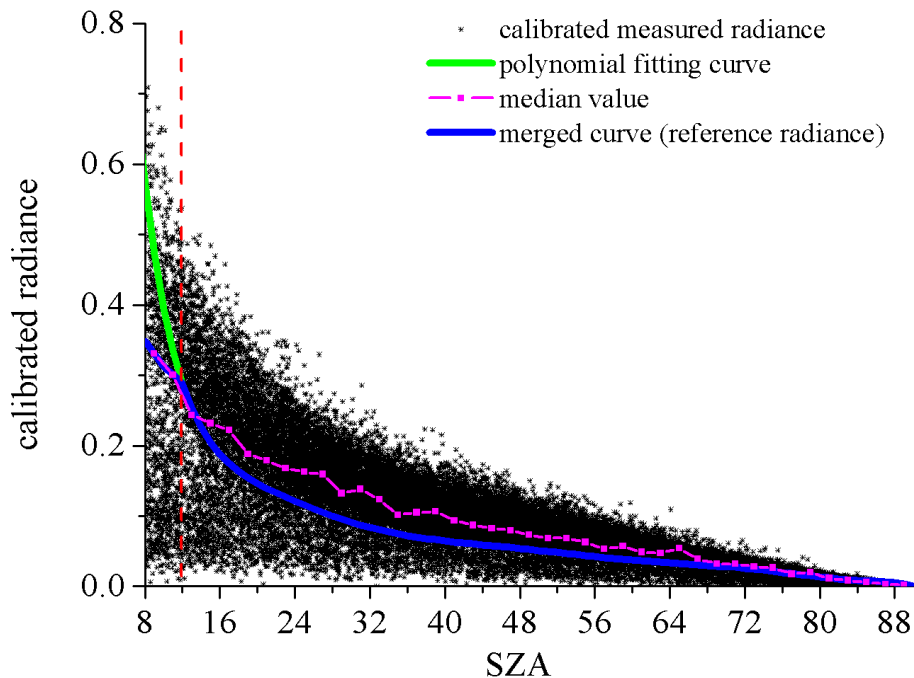


**Figure 4.** Calibrated radiances at 380 nm (black points) extracted from all measurements in the whole period. The blue curve represents a merged clear sky reference values over the whole SZA range (8–90°): above 81° it is based on radiative simulation results; between 12 and 81° it represents a polynomial fit to the clear sky measurements shown in Fig. 8b; below 12° it is determined by calculating the median value of the measured radiance (see text). The green curve represents the extension of the polynomial fit to SZA < 12°. The magenta curve represents the median values of the measured radiance. The red dashed line presents the SZA of 12°.

**Cloud and aerosol classification for 2 1/2 years of MAX-DOAS observations**

Y. Wang et al.

Title Page	
Abstract	Introduction
Conclusions	References
Tables	Figures
◀	▶
◀	▶
Back	Close
Full Screen / Esc	
Printer-friendly Version	
Interactive Discussion	



## Cloud and aerosol classification for 2 1/2 years of MAX-DOAS observations

Y. Wang et al.

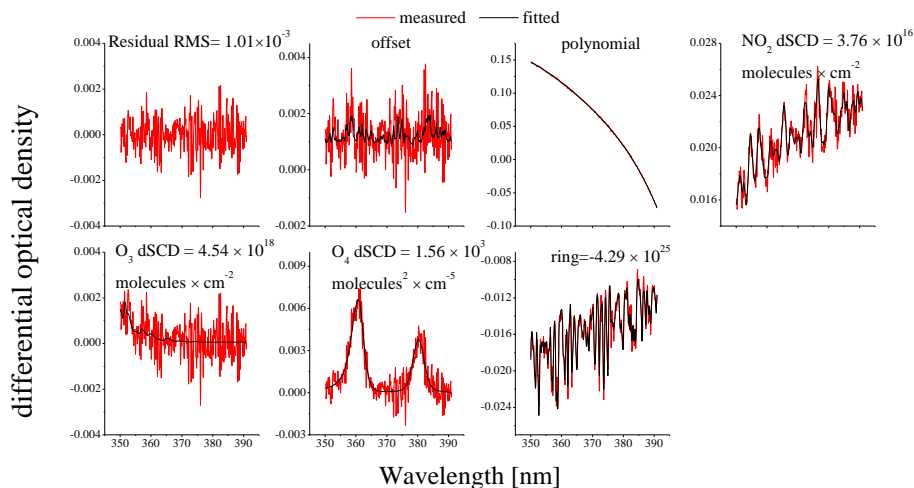


**Figure 5.** Example of a DOAS fit for a spectrum measured at an elevation angle of  $5^\circ$  at 11:47 LT on 15 September 2012 using the FRS from the same elevation sequence. The red lines indicate the trace gas cross sections scaled to the corresponding absorptions in the measured spectrum (black); the black lines indicate the respective fit results.

**Cloud and aerosol classification for 2 1/2 years of MAX-DOAS observations**

Y. Wang et al.



**Figure 6.** (a) The black, red and blue curves indicate the time series and the corresponding SZA of original  $CI_z$ , reference  $CI_z$  and normalised  $CI_z$ , respectively, on 8 July 2012. The dashed line presents the threshold of normalised  $CI$  of 0.84. The visual images in the morning (b) and in the afternoon (c) from MODIS are over the Wuxi site on the day.

Title Page

Abstract

Introduction

Conclusions

References

Tables

Figures

◀

▶

◀

▶

Back

Close

Full Screen / Esc

Printer-friendly Version

Interactive Discussion

## Cloud and aerosol classification for 2 1/2 years of MAX-DOAS observations

Y. Wang et al.

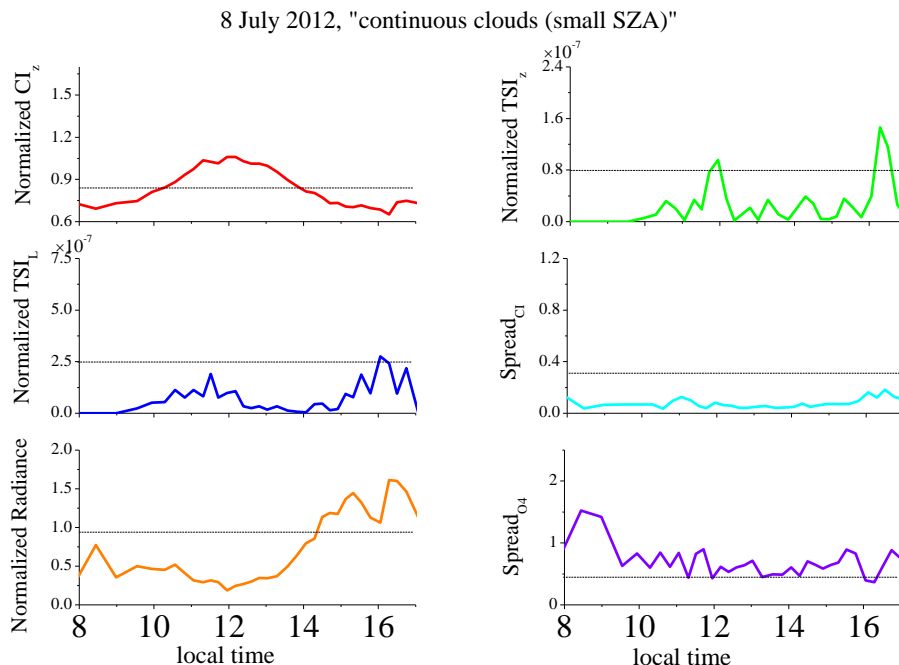


**Figure 7.** Time series of the quantities derived from MAX-DOAS for 8 July 2012, categorized as “continuous clouds (small SZA)”. While around noon the normalised CI indicates clear sky, the spread of the CI and the normalised radiance indicate the presence of clouds. The dashed line presents the thresholds of each quantity.

Title Page

Abstract

Introduction

Conclusions

References

Tables

Figures

◀

▶

◀

▶

Back

Close

Full Screen / Esc

Printer-friendly Version

Interactive Discussion



## Cloud and aerosol classification for 2 1/2 years of MAX-DOAS observations

Y. Wang et al.

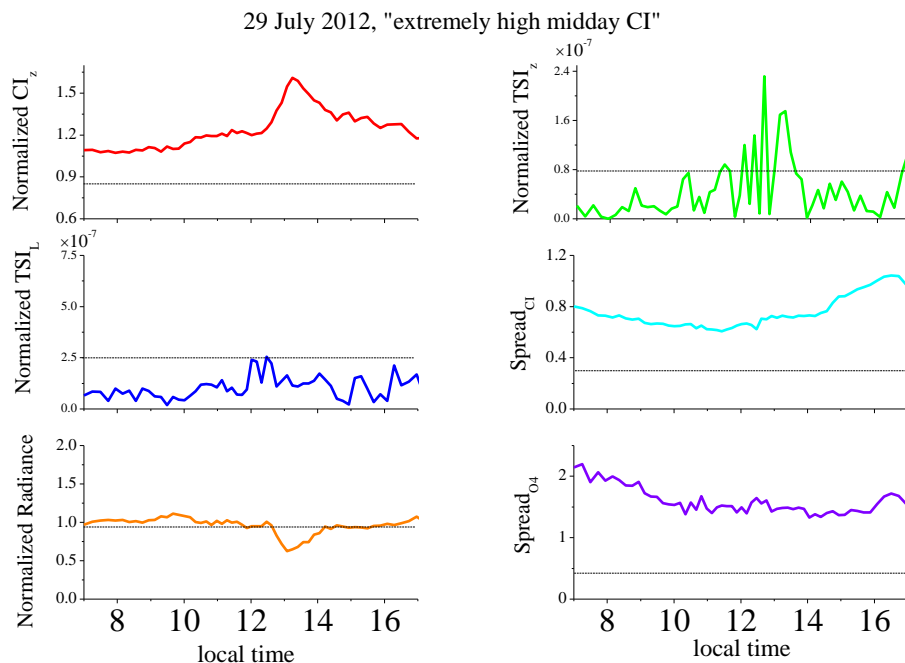


**Figure 8.** Time series of the quantities derived from MAX-DOAS for clouds classification on 29 July 2012, categorized as “extremely high midday CI”. The dashed line presents the thresholds of each quantities.

## Cloud and aerosol classification for 2 1/2 years of MAX-DOAS observations

Y. Wang et al.

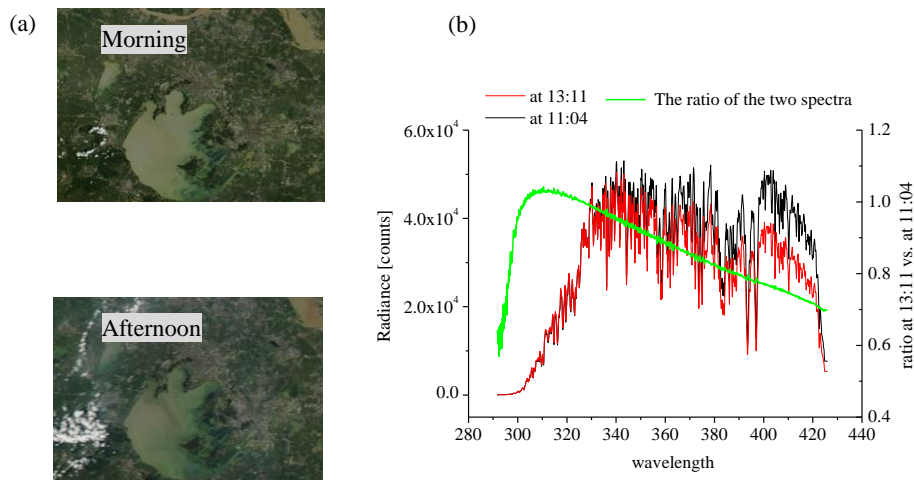


**Figure 9.** (a) visual images of MODIS on 29 July 2012 with the sky condition of “extremely high midday CI”; (b) zenith spectra in the morning (black) and afternoon (red) measured at a SZA of 20°. The green curve indicates the ratio of the spectrum in the morning against in the afternoon.

Title Page

Abstract

Introduction

Conclusions

References

Tables

Figures

◀

▶

◀

▶

Back

Close

Full Screen / Esc

Printer-friendly Version

Interactive Discussion

## Cloud and aerosol classification for 2 1/2 years of MAX-DOAS observations

Y. Wang et al.

■ clear with low aerosol    ■ extremely high midday CI    ■ clear with high aerosol  
■ zenith cloud holes    ■ off-zenith cloud holes    ■ broken clouds    ■ continuous clouds (large SZA)  
■ continuous clouds (small SZA)    ■ fog    ■ optically thick clouds

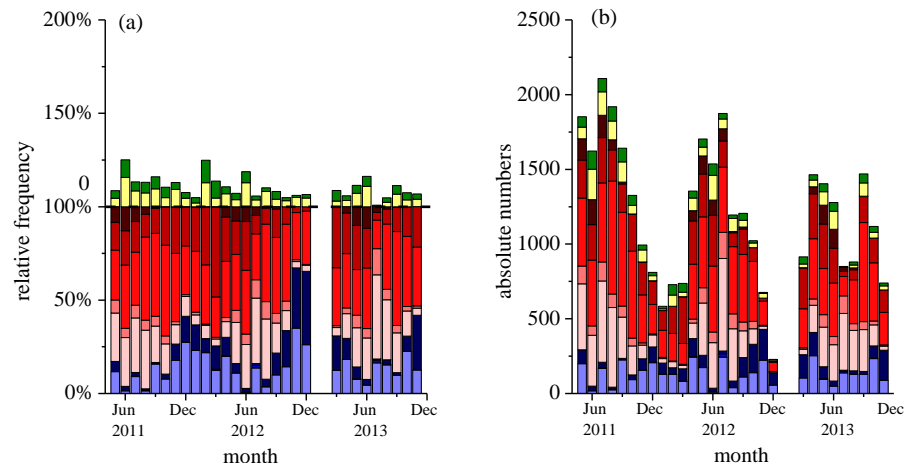


**Figure 10.** The monthly frequency distribution of the cloud classification scheme. **(a)** Relative frequencies of the different sky conditions (indicated by the different colors). Bars between 0 and 100 % represent the frequency of the primary sky conditions; bars above 100 % represent the frequency of the secondary sky conditions. The black dashed line represents emphasizes the 100 % mark. **(b)** Accumulated absolute numbers of the sky conditions in each month.

## Cloud and aerosol classification for 2 1/2 years of MAX-DOAS observations

Y. Wang et al.

■ clear with low aerosol   
 ■ extremely high midday CI   
 ■ clear with high aerosol  
■ zenith cloud holes   
 ■ off-zenith cloud holes   
 ■ broken clouds   
 ■ continuous clouds (large SZA)  
■ continuous clouds (small SZA)   
 ■ fog   
 ■

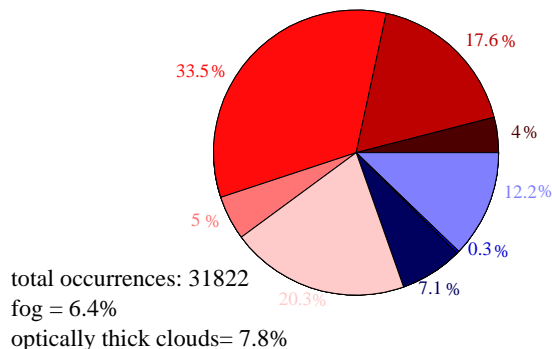


**Figure 11.** Relative fractions of the different sky conditions retrieved from the MAX-DOAS cloud classification scheme during the whole measurement period.

Title Page	
Abstract	Introduction
Conclusions	References
Tables	Figures
◀	▶
◀	▶
Back	Close
Full Screen / Esc	
Printer-friendly Version	
Interactive Discussion	



## Cloud and aerosol classification for 2 1/2 years of MAX-DOAS observations

Y. Wang et al.

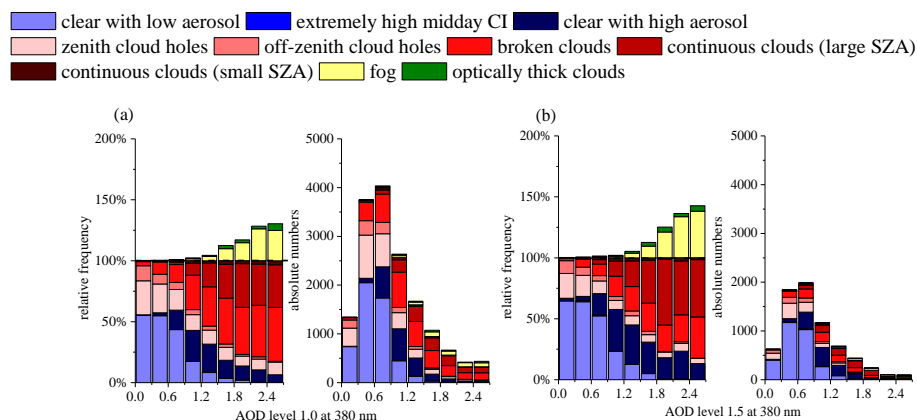


**Figure 12.** Results of the cloud classification scheme as a function of the AOD obtained from the AERONET measurements at Taihu. **(a)** The AOD is from the level 1.0 data sets without cloud-screening and **(b)** from automatically cloud cleared level 1.5 data sets. In each subfigure, left: relative frequencies of the different sky conditions, see the caption of Fig. 10 and the text for details; right: absolute numbers of the sky conditions as function of the AOD.

## Cloud and aerosol classification for 2 1/2 years of MAX-DOAS observations

Y. Wang et al.

■ clear with low aerosol   
 ■ extremely high midday CI   
 ■ clear with high aerosol  
■ zenith cloud holes   
 ■ off-zenith cloud holes   
 ■ broken clouds   
 ■ continuous clouds (large SZA)  
■ continuous clouds (small SZA)   
 ■ fog   
 ■ optically thick clouds

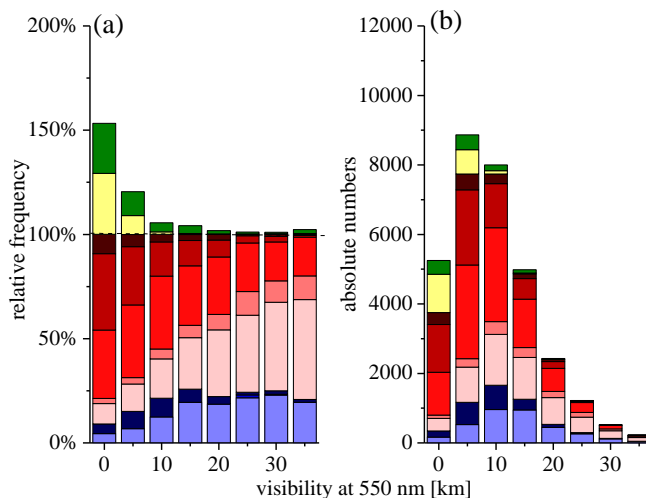


**Figure 13.** Results of the cloud classification scheme as a function of the visibility at 550 nm obtained from the visibility meter. **(a)** Relative frequencies of the different sky conditions (see the caption of Fig. 10). **(b)** Absolute numbers of the sky conditions as a function of the visibility.

Title Page

Abstract Introduction

Conclusions References

Tables Figures

◀ ▶

◀ ▶

Back Close

Full Screen / Esc

Printer-friendly Version

Interactive Discussion



## Cloud and aerosol classification for 2 1/2 years of MAX-DOAS observations

Y. Wang et al.

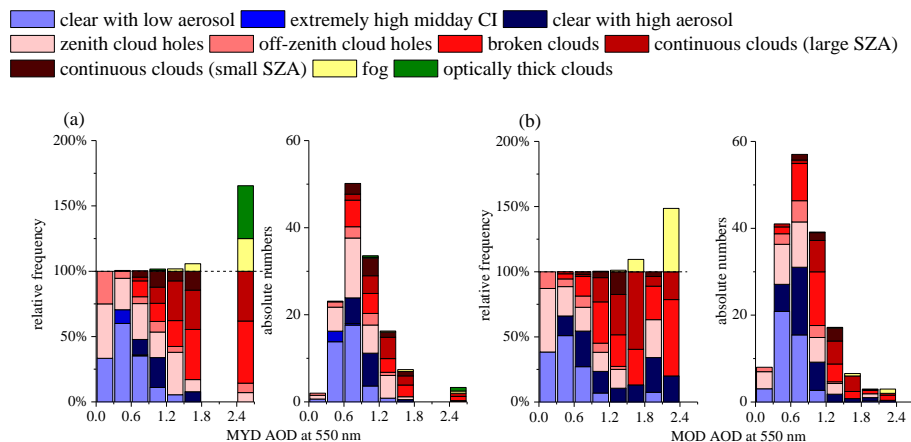


**Figure 14.** Results of the cloud classification scheme as a function of the aerosol optical depth (AOD) at 550 nm from MODIS on Aqua (MYD) **(a)** and on Terra (MOD) **(b)**. The left parts of the figures present the relative frequencies of the different sky conditions (see the caption of Fig. 10). The right parts of the figures present the absolute numbers of the sky conditions.

Title Page

Abstract

Introduction

Conclusions

References

Tables

Figures

◀

▶

◀

▶

Back

Close

Full Screen / Esc

Printer-friendly Version

Interactive Discussion



## Cloud and aerosol classification for 2 1/2 years of MAX-DOAS observations

Y. Wang et al.

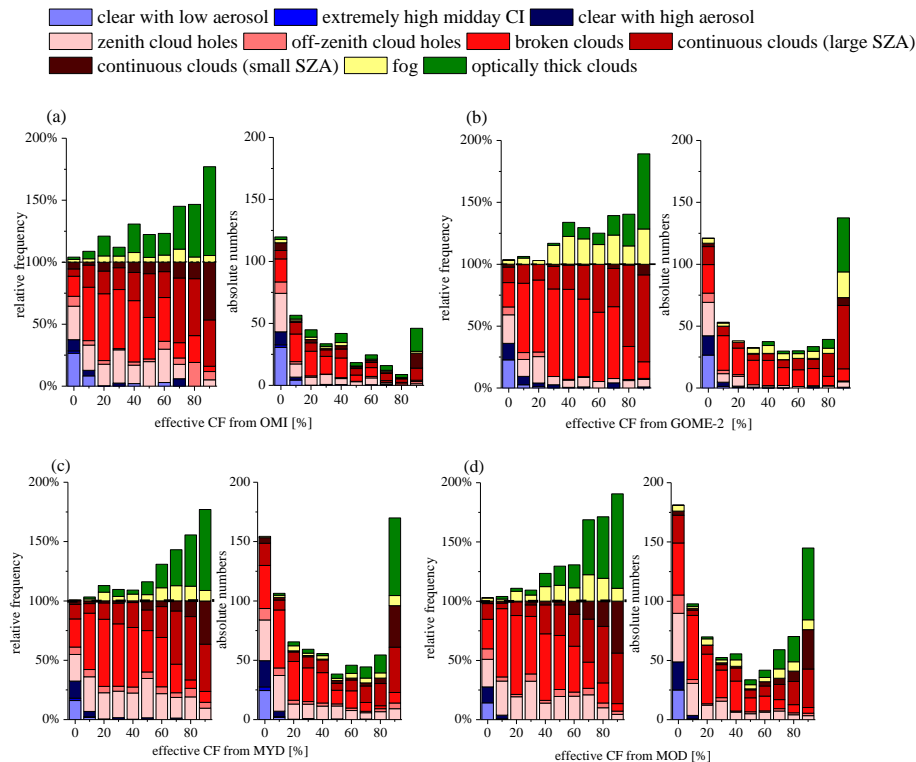


**Figure 15.** Results of the cloud classification scheme as a function of effective cloud fractions derived from (a) OMI, (b) GOME-2, (c) MODIS on Aqua (MYD), (d) MODIS on Terra (MOD). The left parts of the figures present the relative frequencies of the different sky conditions (see the caption of Fig. 10). The right parts of the figures present the absolute numbers of the sky conditions.

## Cloud and aerosol classification for 2 1/2 years of MAX-DOAS observations

Y. Wang et al.

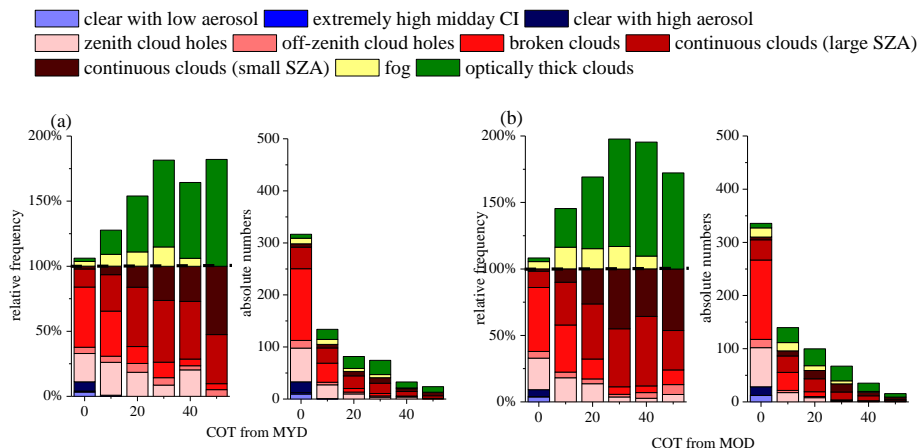


**Figure 16.** Results of the cloud classification scheme as a function of the cloud optical thickness (COT) from MODIS on Aqua (MYD) **(a)** and on Terra (MOD) **(b)**, both for measurements with geometrical CF > 80 % only. The left parts of the figures present the relative frequencies of the different sky conditions (see the caption of Fig. 10). The right parts of the figures present the absolute numbers of the sky conditions.

Title Page

Abstract

Introduction

Conclusions

References

Tables

Figures

◀

▶

◀

▶

Back

Close

Full Screen / Esc

Printer-friendly Version

Interactive Discussion

## Cloud and aerosol classification for 2 1/2 years of MAX-DOAS observations

Y. Wang et al.

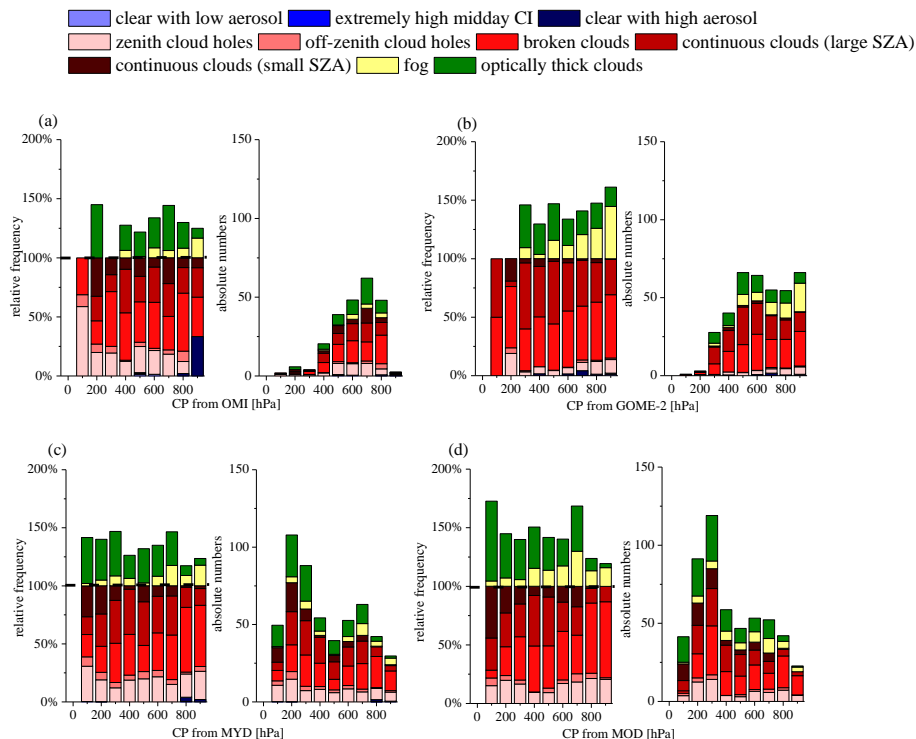


**Figure 17.** Results of the cloud classification scheme as a function of cloud pressure derived from different satellite observations for effective cloud fraction above 0.2: cloud pressure from (a) OMI, (b) GOME-2, (c) MODIS on Aqua, (d) MODIS on Terra. The left parts of the figures present the relative frequencies of the different sky conditions (see the caption of Fig. 10). The right parts of the figures present the absolute numbers of the sky conditions.

Title Page

Abstract

Introduction

Conclusions

References

Tables

Figures

◀

▶

◀

▶

Back

Close

Full Screen / Esc

Printer-friendly Version

Interactive Discussion

## Cloud and aerosol classification for 2 1/2 years of MAX-DOAS observations

Y. Wang et al.

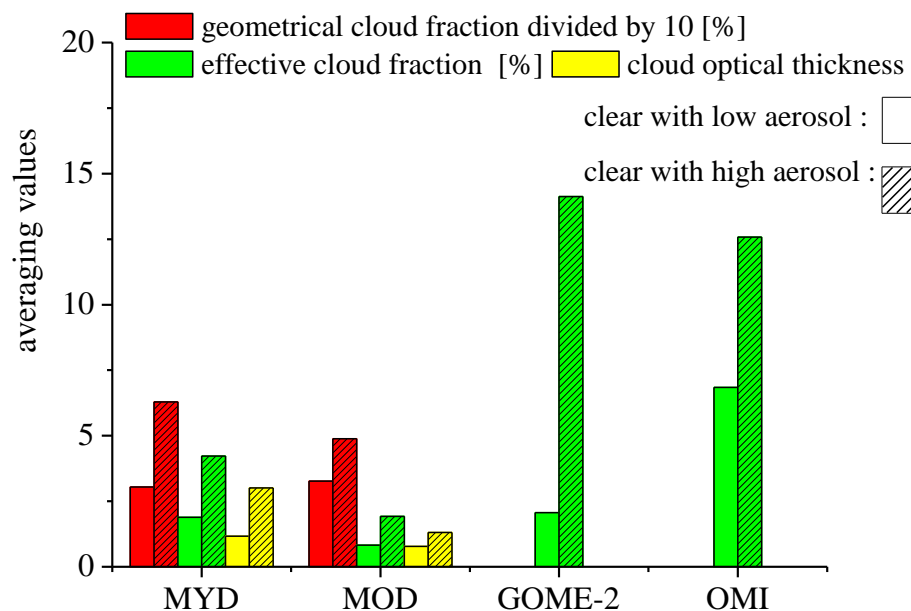


**Figure 18.** Average values of various cloud properties (indicated by the different colors) derived from the MODIS on Aqua (MYD) and on Terra (MOD) as well as GOME-2 and OMI for clear sky conditions with low or high aerosols (as identified by MAX-DOAS). The open bars and hatched bars represent clear sky conditions with low aerosol and high aerosol load, respectively. The geometrical cloud fractions are divided by 10.

Title Page

Abstract

Introduction

Conclusions

References

Tables

Figures

◀

▶

◀

▶

Back

Close

Full Screen / Esc

Printer-friendly Version

Interactive Discussion